AD 255 858

Prof. Dr. Hans M e i n k e
Institut für Hochfrequenztechnik
der Technischen Hochschule München

Research on broadband antenna design

Final report

Contract No. AF 61 (052) - 41

The research reported in this document has been sponsored by the

Wright Air Development Center

of the Air Research and Development Command, United States Air Force, through its European Office under contract AF (052) - 41

Summary:

Four technical notes concerning the development of a broad-band omnidirectional antenna, with as many frequency independent electrical characteristics as possible, have been written by us to-date.

The first part of this final report gives a review of the contents of earlier reports.

Part two is a summary of all the usable measures that decrease the frequency dependence of the radiation pattern of broad-band radiators. In addition to the already mentioned radiator shapes with dielectric, two further technically important antenna shapes will be described in detail. These are:

1. a 50 ohm radiator, with good broad-band matching, having a broad-band diffused radiation pattern which resembles that of a short dipole over a large frequency range.
2. a 60 ohm radiator that has a constant horizontal direction for the main lobe and also a good broad-band matching.

Part three describes the theoretical advances. The shape of a broad-band radiator is not critical in the vicinity of its vertex; in particular, the electrical characteristics are practically unchanged when a conducting cone, having a small aperture angle and infinite length is set on top of the radiator.

Upon taking these facts into consideration, we developed a new coordinate system for the 60 ohm spherical radiator which has the advantage over the preciously used system that the values F_n and G_n remain finite, even at the radiator apex.

Summary:

Four technical notes concerning the development of a broad-band omnidirectional antenna, with as many frequency independent electrical characteristics as possible, have been written by us to-date.

The first part of this final report gives a review of the contents of earlier reports.

Part two is a summary of all the usable measures that decrease the frequency dependence of the radiation pattern of broad-band radiators. In addition to the already mentioned radiator shapes with dielectric, two further technically important antenna shapes will be described in detail. These are:

1. a 50 ohm radiator, with good broad-band matching, having a broad-band diffused radiation pattern which resembles that of a short dipole over a large frequency range.
2. a 60 ohm radiator that has a constant horizontal direction for the main lobe and also a good broad-band matching.

Part three describes the theoretical advances. The shape of a broad-band radiator is not critical in the vicinity of its vertex; in particular, the electrical characteristics are practically unchanged when a conducting cone, having a small aperture angle and infinite length is set on top of the radiator.

Upon taking these facts into consideration, we developed a new coordinate system for the 60 ohm spherical radiator which has the advantage over the preciously used system that the values F_n and G_n remain finite, even at the radiator apex.

to the radiator, as calculated in the first report, definitely gives broad-band matching. However, small variations in the transition region, from that of the ideal shape, already give noticeable mismatching. Therefore the theory of the feeding zone construction is confirmed.

The measured impedance curves of six different antenna shapes give information about the influence of the radiator shape on the input impedance of the antenna; once the previously analyzed feeding zone considered as the correct one, is always referred to.

The matching improves as the radiator departs more and more form its slim shape, and approaches a sphere-like construction. All six antenna shapes considered indicate high pass characteristics, that is: their mismatching decreases as the frequency is increased. The sphere-like radiator is almost completely matched above a low frequency limit.

Technical Note No. 2

The technical application of the broad-band radiator depends considerably upon whether the continuous, by existing frequency dependence of the radiated pattern can be kept sufficiently small in the large frequency range where impedance matching is obtained. Therefore, the causes of this frequency dependence will be determined next and then measures can be derived which can control this frequency dependence.

The wave separation process of such radiators, and especially the current distribution along the radiator, will be closely analyzed in a theoretical manner.

The measured radiation patterns for four different radiator shapes follow. The relatively small frequency dependence of the diagram in respect to the broad-band impedance characteristics will be explained on the basis of the previously calculated current distribution.

The investigation of the other causes for frequency dependence gave satisfactory results. It was found that the main cause of frequency dependence was removed when dielectric rings were inserted about the feeding zone. The direction of the main lobe now remains constant over a frequency range of 1 : 15, and the side lobes are small.

Technical Note No. 4

Our investigations of the input impedance and radiation pattern of broad-band antennas were conducted only on antennas which were designed for connection to a 60 ohm coaxial cable. The results obtained are certainly so general that they will also yield the optimum radiator shape when an input line having a different characteristic impedance is used. Note No. 4 describes the shape and the electrical characteristics of a constructed broad-band omnidirectional antenna, which is matched [illegible] 60 ohm coaxial cable

[illegible] the reflection factor has [illegible] a steep downward slope at a [illegible] and remains almost completely [illegible] the characteristic impedance of the input line.

The construction drawings show the geometrical dimensions of the radiator and the transition from the outer conductor of the input line to the broad plane.

Part 2: Decreased Frequency Dependence of the Radiation Patterns of Broad-band Omnidirectional Radiators

All applications of antennas for wider frequency bands have demonstrated the fact, that the radiation pattern's frequency dependence is very disturbing. Now that it has been possible to construct a broad band radiator whose input impedance remains matched to the input line over a wide frequency range [illegible] special significance since the [illegible] large frequency dependence in this large frequency range [3. 4]. Therefore the technical appli-

cation of such antennas certainly presents a problem. Thus, the search for a method which decreases the frequency dependence of a broad-band radiator is unavoidable.

The theory of the wide-band radiator [1, 3, 5] shows that a radiator transmits space waves of different modes and these space waves are combined in the radiation pattern in respect to frequency dependent phase shifts. The ideal wide-band radiator would be the one which transmits only one mode type at all frequencies and therefore, always shows the radiation pattern of this mode. The theory indicates that the excitation of a mode type is dependent upon the inhomogeneous characteristics of the vicinity of the radiator [5]. This inhomogenity usually comes from the use of a curved surface radiator. It is very difficult to answer the question, is there a radiator shape that theoretically transmits only one mode type in a wide frequency range. Since we have investigated numerous field patterns, we can conclude with considerable assurance, that the existance of such an ideal radiator is somewhat impossible. However, it cannot be denied that the mode types are noticeably affected if inhomogenous dielectric, whose dielectric constant is dependent on its position, is inserted in the direct vicinity of the antenna. The fields of waves resulting from the use of such dielectric are extremely difficult to analyze and have rarely been analyzed theoretically. Therefore, general and reliable information in this respect, is not available. However it does not seem to be completely impossible that such an antenna in a special dielectric material could be designed and have the capability of generating one frequency independent mode type. However the practical realization would probably result in failure since the dielectric would have to extend out to infinity.

One can still influence the radiation pattern considerably by using inhomogeneous dielectric with finite dimensions and thus find radiation patterns which have practical and interesting shapes. For example, it is known that a control of the

radiation pattern is possible by means of dielectric rings and in this manner an almost frequency independent main lobe direction and very small side lobe maximums are obtained [3] . Also, the only frequency dependence in this case, is the decrease in the 50 % down bandwidth of the main lobe as the frequency increases. This would be a radiator having very good horizontal directivity. Also it is possible to find a diagram which is very similar, over a large frequency range, to that of a short dipole. This would be a radiator suitable for uniform transmission of waves about a large radial sector and is also suitable for reception of waves progressing radially through this area. In the following, the basic rules showing the influence on the radiation pattern by means of dielectric, as well as the most important technical shapes, will be treated.

I. The Radiation Patterns of Simple Broad-band Radiators

Radiators which are energized out of the ground plane by means of a coaxial line, as shown in Figure 1, will be treated here. Their shape begins at the feeding-zone with a cone, whose characteristic impedance in respect to the ground plane, is the same as that of the coaxial input line. Then the form transfers over to a final rounded shape. In the following, a simple method which is suitable for approximate calculation of the radiation pattern will be explained. This approach is sufficient to clarify the existance of distant fields and is an aid in developing suitable measures for decreasing the frequency dependence of the radiation pattern.

According to [5] , the wavefronts near the radiator itself, are approximated by the static field lines of an electric field between the radiator and the ground plane. Such wavefronts are shown in Figure 1. The current along the radiators of good wide-band antennas, decreases rapidly from the input point to the upper end as shown in [3] . Practically no current flows in the upper end of the radiator and thus contributes

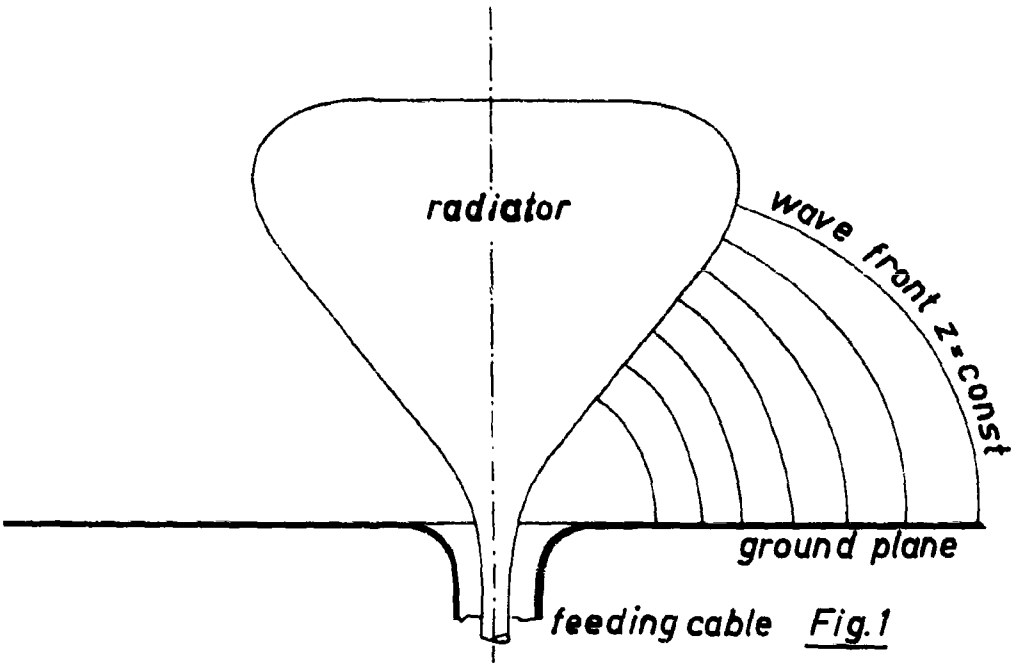
radiator
wave front z=const
ground plane
feeding cable

Fig.1

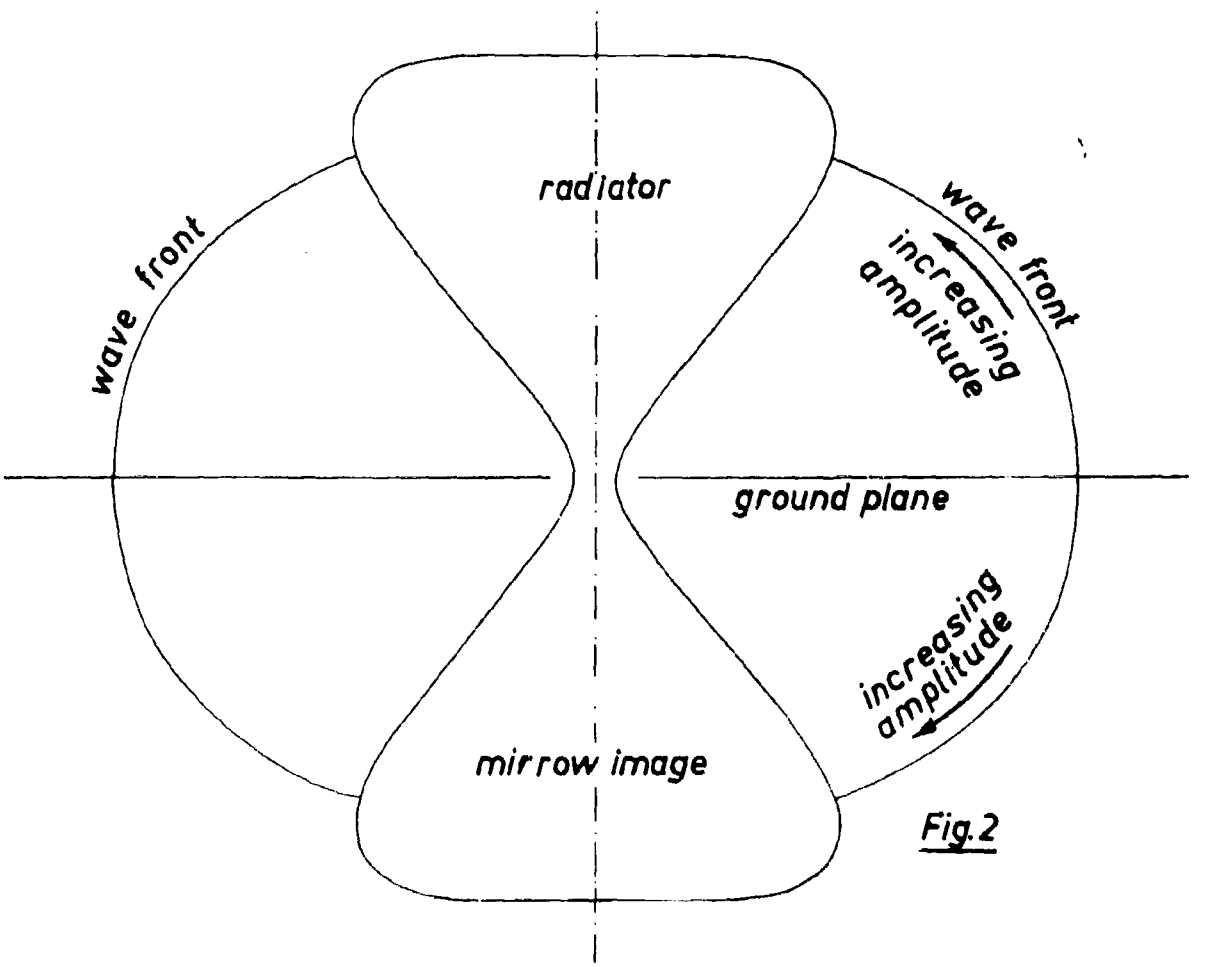
radiator
wave front
wave front
increasing amplitude
ground plane
increasing amplitude
mirrow image

Fig.2

little toward radiation. The wave propagation from the antenna is almost completely composed of that shown in Figure 1, resulting from the wavefront of the existing waves. In accordance with the "Huygens Principle" [6], each point of a wavefront can be considered as a center of secondary waves, whereby the distant field of the radiator can be approximated as the sum of secondary waves, for example: those which propagate from the outer most wavefront shown in Fig.1. One can postulate that the points of these static field lines are equivalent to in-phase generators. However, this wavefront is not uniform in respect to amplitude, rather, the amplitude increases from the ground plane to the radiator, since the electric field lines have a smaller displacement at the radiator than at the ground plane and this results in a larger electric field intensity near the radiator. The effectiveness of the ground plane can usually be determined by adding the mirrow image of the radiator. Therefore one considers the symmetrical arrangement of Fig.2. The distant field of the radiator is then approximated from the cylindrical symmetry of the wavefront in Fig.2.

In Fig.3, the curves "a" show the radiation patterns of the antenna of Fig.1, whose input line has a characteristic impedance of 60 ohms. Fig. 4 shows two of the curves from Fig.3, with the symmetrical complement at the bottom. These curves result from the wavefront of Fig.2 and can be approximated mathematically by using the "Huygens Principle". The effect shown in Fig.3 and 4 is known to exist in similar form in funnel radiators. The curvature of the resulting wavefront brings a broadening of the main lobe maximum at lower frequencies, and increasing frequency & increasing curvature results in a splitting of the main lobe into two or more maxima, as shown in Fig. 4b [7, 8]. The curvature also prevents the radiation pattern minima from reaching zero. Zero minima are obtained with excitation via even, uniform phase fronts. However, the minima are always less pronounced with increased

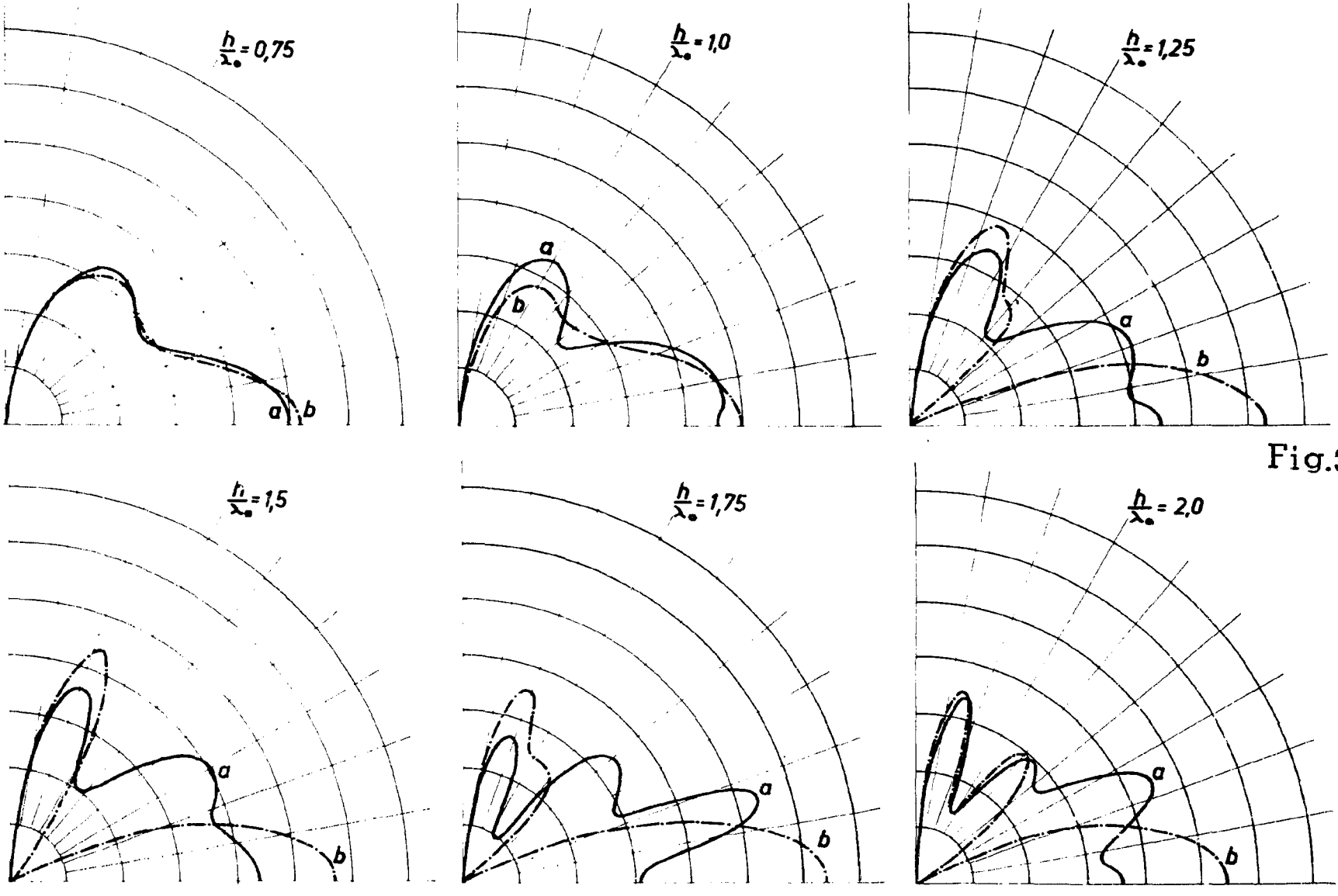
$\frac{h}{\lambda_0} = 0{,}75$
a
b
$\frac{h}{\lambda_0} = 1{,}0$
a
b
$\frac{h}{\lambda_0} = 1{,}25$
a
b
$\frac{h}{\lambda_0} = 1{,}5$
a
b
$\frac{h}{\lambda_0} = 1{,}75$
a
b
$\frac{h}{\lambda_0} = 2{,}0$
a
b

Fig.3

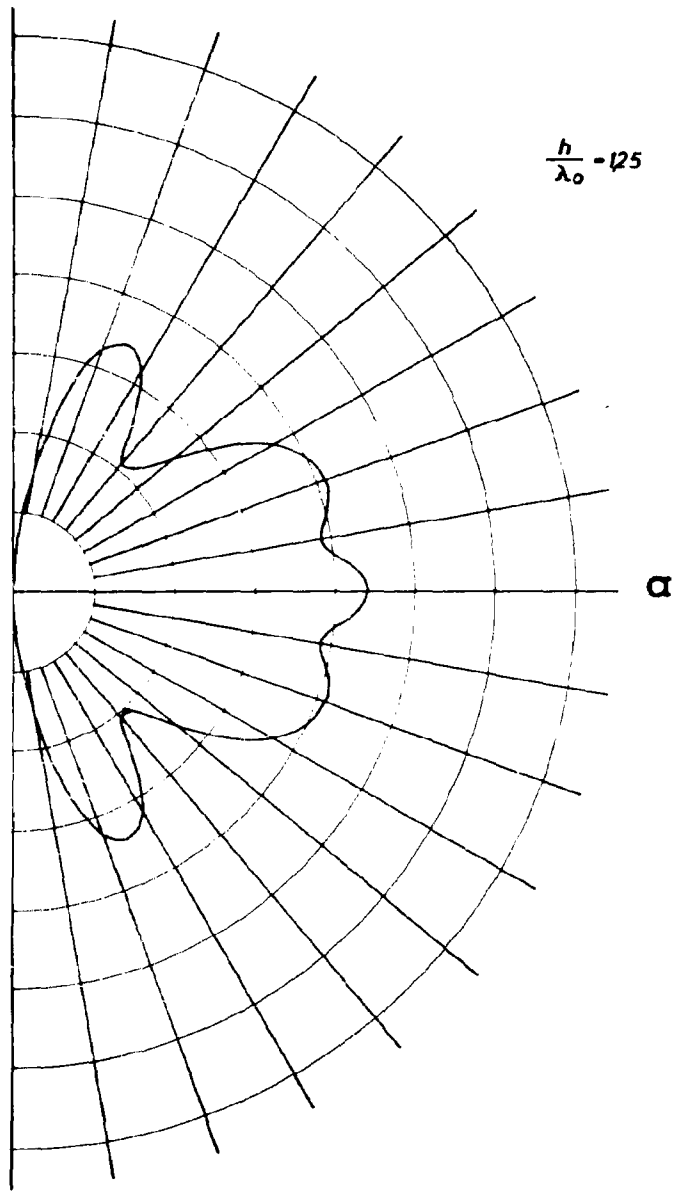

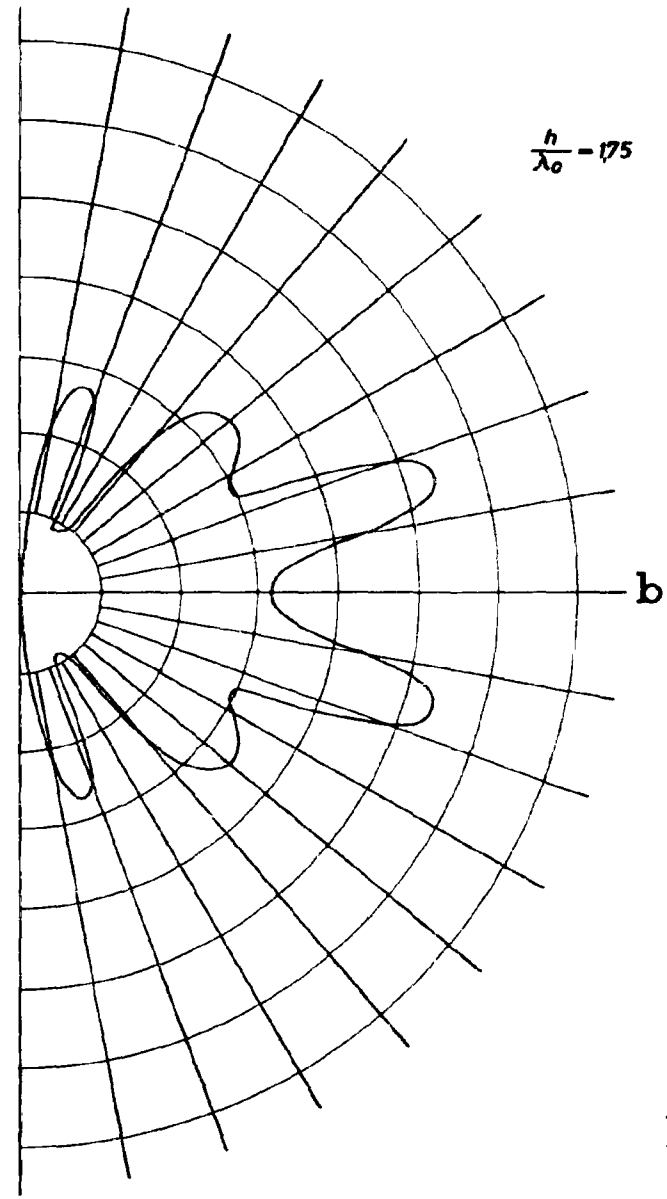

Fig.4

curvature [9, 10] . In addition, the side lobes become larger with increasing amplitude of the wavefront, as the radiator surface is approached, and can becomes larger than the main lobe maximum as shown in Fig.4, with sufficiently increasing high frequency, when the border radiation of the wavefront is large.

II. Measures to Concentrate the Main Lobe Maximum

The undesired broadening or splitting of the main lobe maximum can be avoided by making the radiating wavefront of Fig.2, as even as possible. The proper measures required are known from the theory of flat radiators. The radiated wavefront in the vicinity of the ground plane, must be drawn back in the direction of the input point by means of a delay arrangement having lense or focusing characteristics. Such a delay can be obtained by using an uneven ground plane; a method which is used in the well known delay line [11] . This method of obtaining delay has only limited applications, since the frequency dependency increases with increasing delay characteristics, and is also effective only in the direct vicinity of the ground plane. A reasonable application of [12] , could be the anticlinal bulging of the ground plane as shown in Fig.5 and this results in a limited effect, such that, the wavefront is drawn back, at least near the ground plane. A larger improvement requires the use of lense arrangements, which are used with funnel radiators. This is necessary since a lense has a continously decreasing effect, as the edge of the wavefront is approached. Therefore the wave is drawn back at all points in a defined and desired manner, such that, they are even throughout (as with a convex lense used for optics). The well known metal lenses, derived from waveguide principles, will not be used for broad-band antennas, since they have a small frequency range. Only dielectric lenses with lossless and frequency independent dielectric will be considered. Such a trolitul lense which has been derived by means of experimen-

tation, is shown in Fig.6. Diagrams of these radiators are shown by the curves "b" of Fig. 3.

These dielectric lenses cause two problems:

- they affect the capacitive distribution along the radiator
- [illegible] the surface of

The altered capacitive distribution produces a different characteristic impedance curve along the radiator. This different characteristic impedance curve is easily corrected to the required wide-band impedance curve by applying small changes to the radiator shape. The reflected component waves at the surface of the lense structure, propagate about the vicinity of the radiator in an undefined manner. These vagabond waves are partially reflected back to the input line and now cause a frequency dependent mismatch. Some of the reflections travel outwards away from the antenna in an undefined manner, and affect the radiation pattern. The trolitul shapes of Figure 6 produce approximately 15 % reflection in the input line. The use of an inhomogeneous dielectric, whose dielectric constant at the edges of the lense possesses a slow and continuous transition from air to dielectric, helps to prevent this type of reflection. Quite a few successful projects were conducted in the U.S.A. in order to produce a dielectric from foam material (synthetic material formed by forcing air through the material in its liquid form) [13]. This dielectric should have a dielectric constant which is a geometrical function. Since the technology of developing such a material is too great, we have used inhomogeneous dielectric and have shown its feasability in the form of a lense consisting of thin trolitul plates with air space in between, as shown in Fig.7. Patterns similar to those of Fig 6 are obtained with this arrangement. In addition, less is reflected to the input line. Therefore better wide-band matching is obtained. The measures mentioned above cause the wavefront to be evened out. This

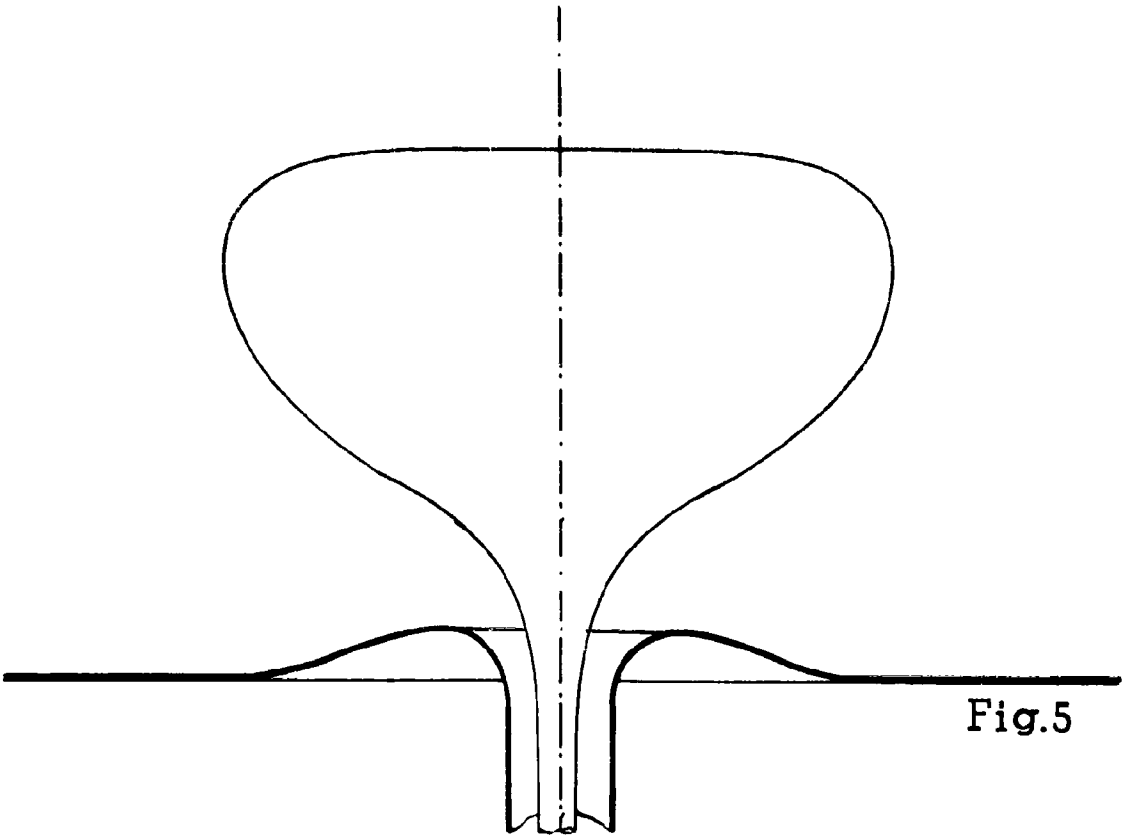

Fig.5

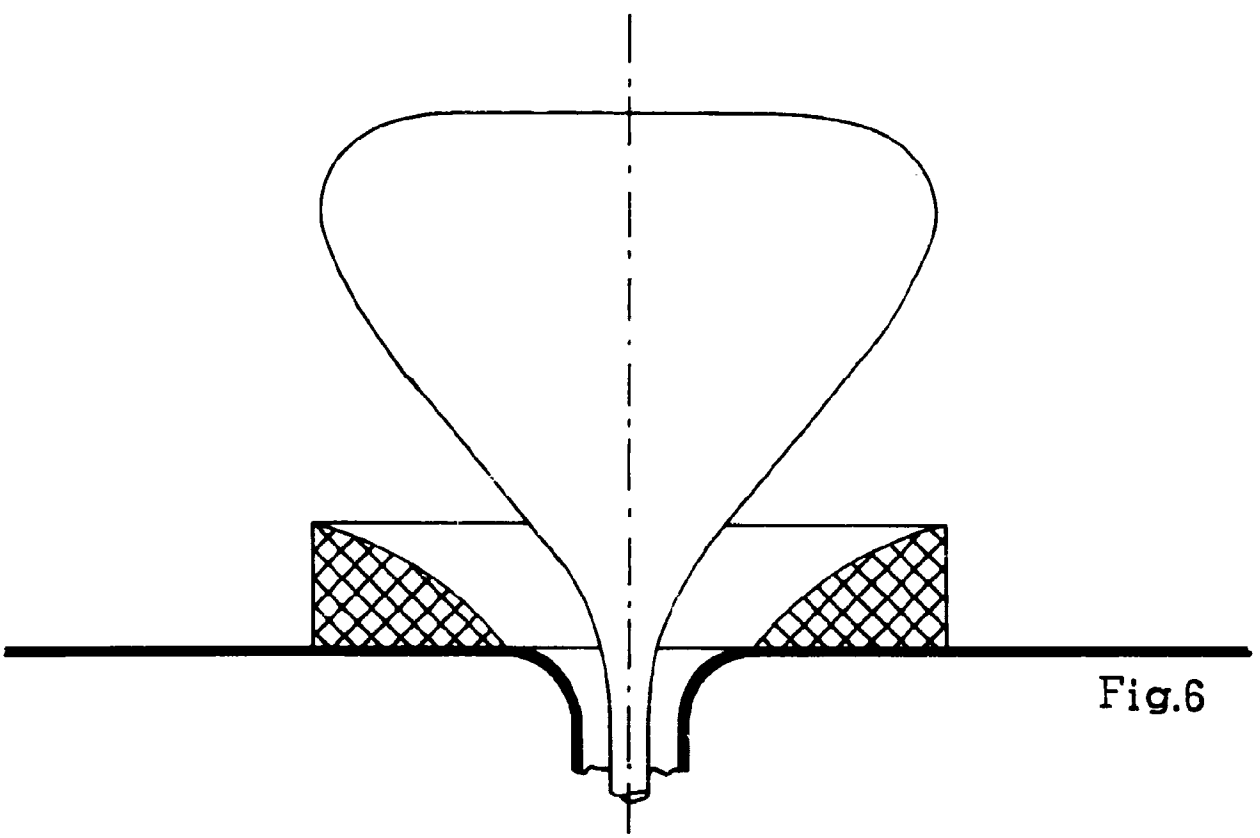

Fig.6

fact is demonstrated by the curves "b" in Fig.3 since the lobe minima are more pronounced and have more nearly approached the characteristics of a true null. The fact that the 50 % down bandwidth of the main lobe decreases with increasing frequency, is clarified, since the vertical broadening of the wavefront (Fig.4) increases, in respect to wavelength, with increasing frequency.

A very simple solution of the dielectric lense without the problem of synthetic foam material, is possible if the input line is filled with dielectric as shown in Fig.8. If one now allows the dielectric of the input line to continue out to the lense as shown in Fig.8, one achieves the condition of no reflections as the wave enters the lense (the contrary is true in Fig.7) and reflected waves are prevented from existing in the cable. The wave leaves the dielectric slowly and continuously, such that a slowly increasing part of the wavefront progresses over to the medium of air. In this way it is possible to obtain the curves b' in Fig.3 with good matching by using a relatively simple piece of solid material.

III. Methods to Decrease the Side Lobes

The curves "b" of Fig.3 show that the only techniques previously mentioned, are ineffective in combating the very large and steep side lobes at high frequencies. These side lobes are caused by the enlarged amplitudes of the edges of the wavefronts and are also possible with even phase fronts. It is known that a reduction in the side lobes in flat radiators also causes an enlarged amplitude in the middle of the radiating surface [9, 14]. Therefore additional methods, the use of which influences the limitation of the phasefront amplitudes, must be found. If the measures taken are to have simple and broad-band characteristics, then this is also accomplished by means of a dielectric lense.

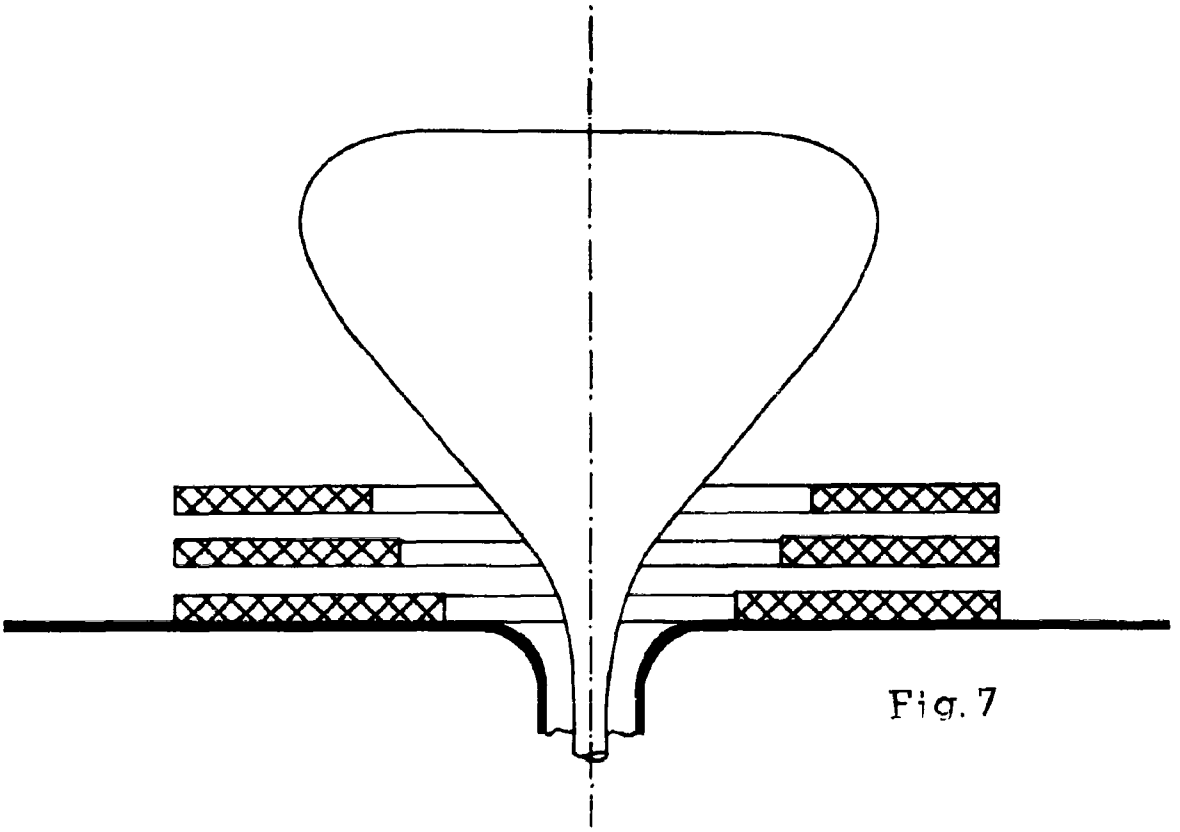

Fig. 7

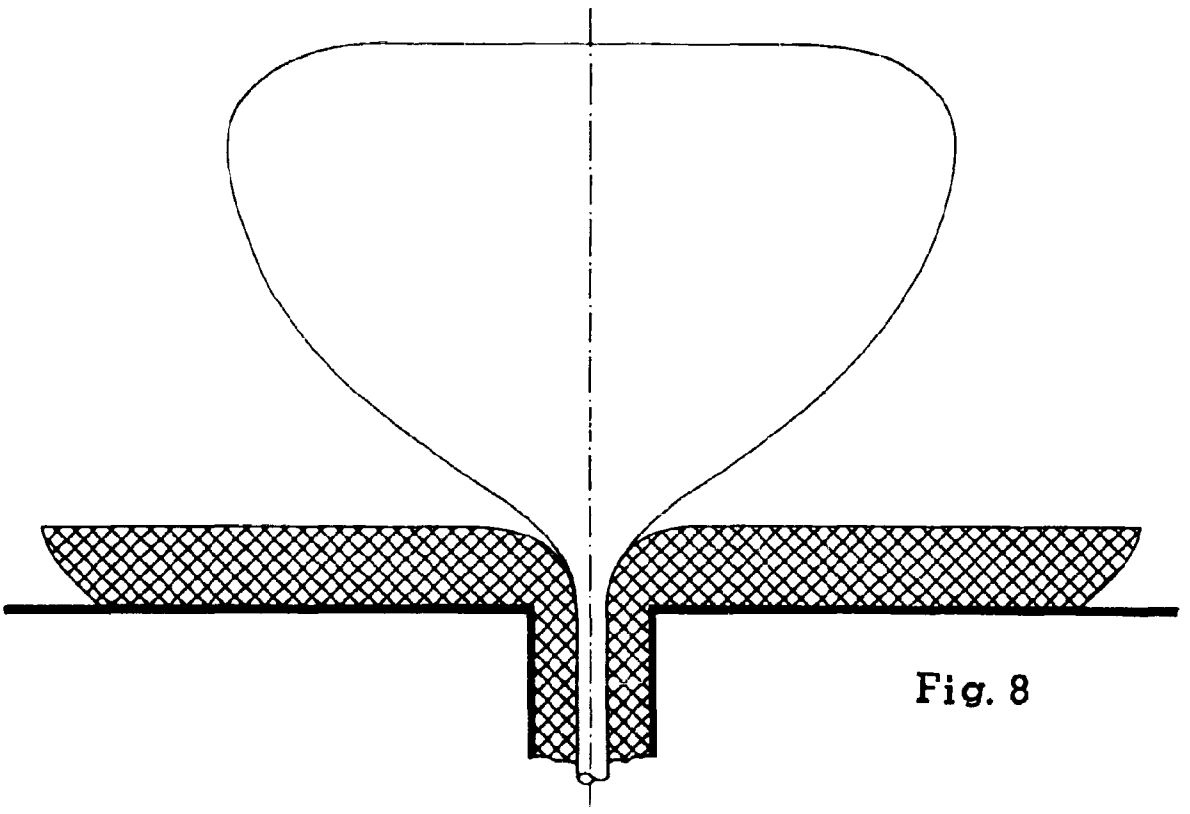

Fig. 8

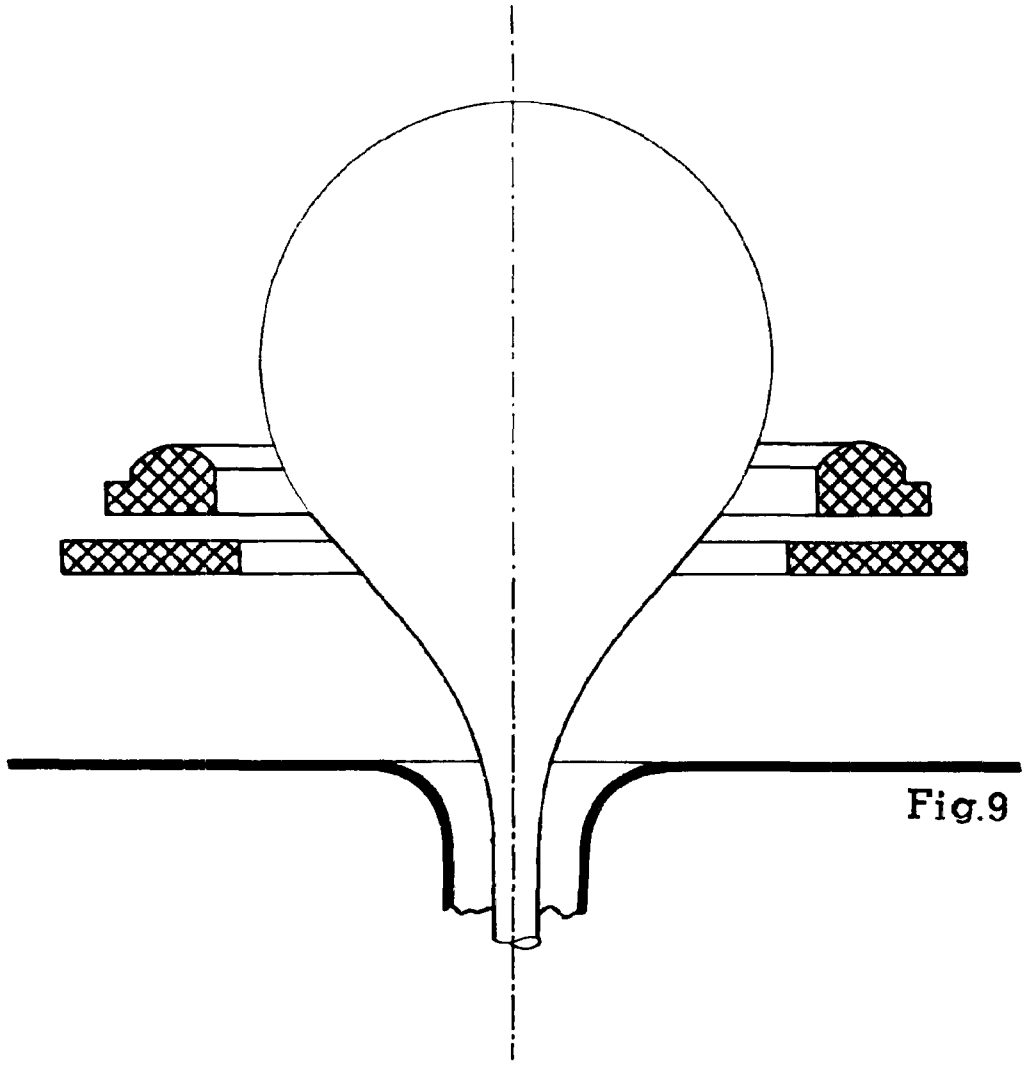

Fig.9

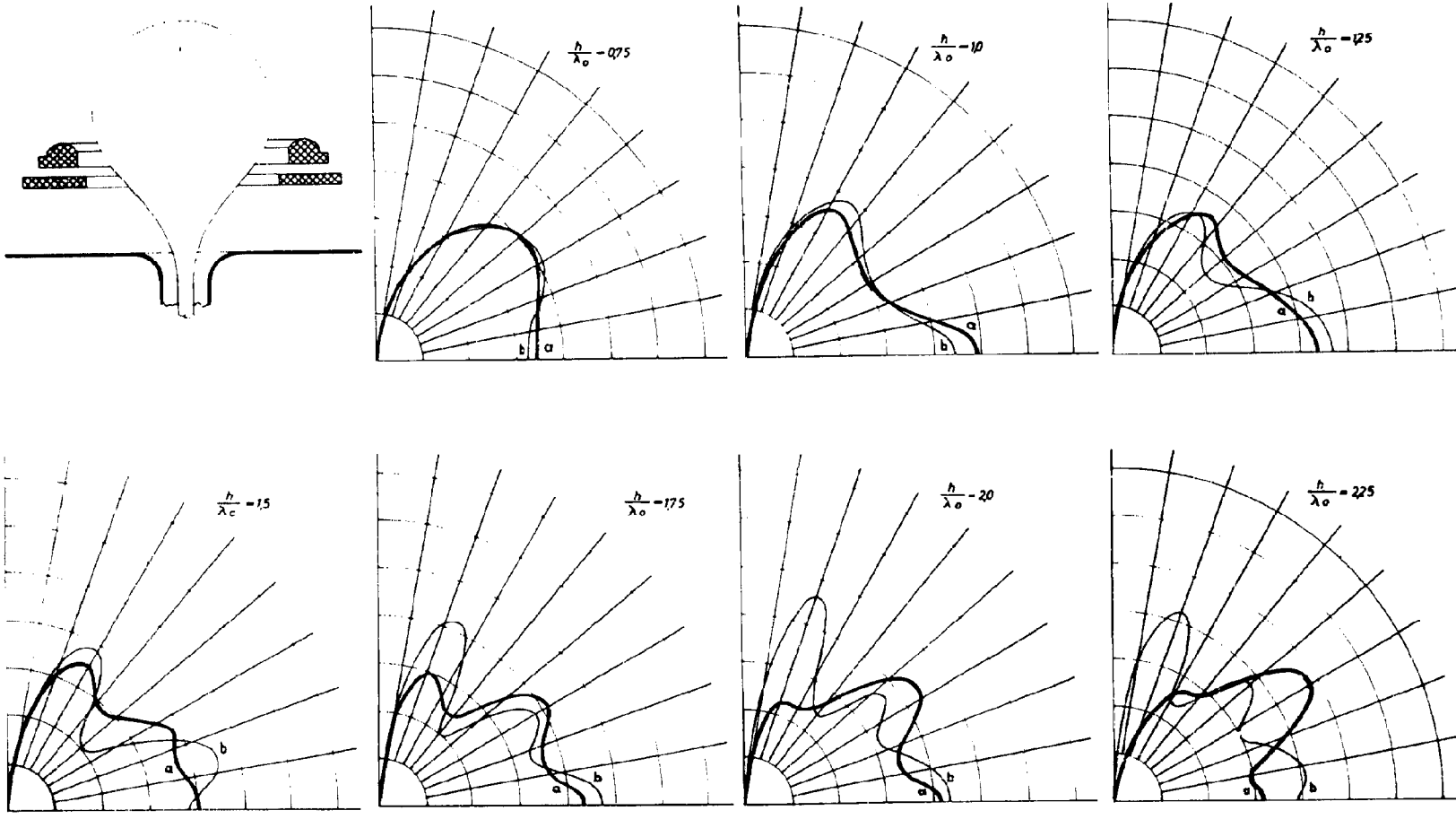

Fig.10

For this reason we constructed a considerable number of dielectric rings of different diameters. Through the combinations of such rings in different arrangements and without air space between rings, we were able to affect the radiation pattern in many ways. If one wishes to reduce the side lobes considerably, then one could, for example, increase the density of the dielectric in specific locations, as shown in Fig.9. Radiation curves "a" as shown in Fig.10. are now obtained. The curves "b" give the radiation pattern of the same radiator without dielectric. One can definitely notice the reduction of the steep side lobes. If one does not use the more conical shaped antenna shown in Fig.1, but uses the more spherical shaped antenna shown in Fig.9, showing a very balanced pattern with very weak minima as indicated, would be quite suitable for transmission and reception in a large angle radial sector.

IV. Wide-band Antenna with Optimum Gain in the Symmetrical Plane

If the phase correction of paragraph II. is combined with the side lobe reduction of paragraph III, one obtains radiation patterns with a well defined main lobe in the symmetrical plane whose angle decreases with increasing frequency. If Fig.7 is combined with a correction, (correction shown by Fig.9), one obtains the optimum shape as shown in Fig.11 and 12 (obtained from simple ring combinations which were experimentally determined). The corresponding radiator patterns are shown in Fig.13. If Fig.8 is combined with the necessary correction, then the shape shown by Fig.14 is the resulting optimum one. Since the dielectric of the input line continues to the lense, the reflection of waves upon entering the lense is avoided, and relatively good impedance matching is achieved. This impedance matching could probably be somewhat improved by very small changes of the lense and radiator

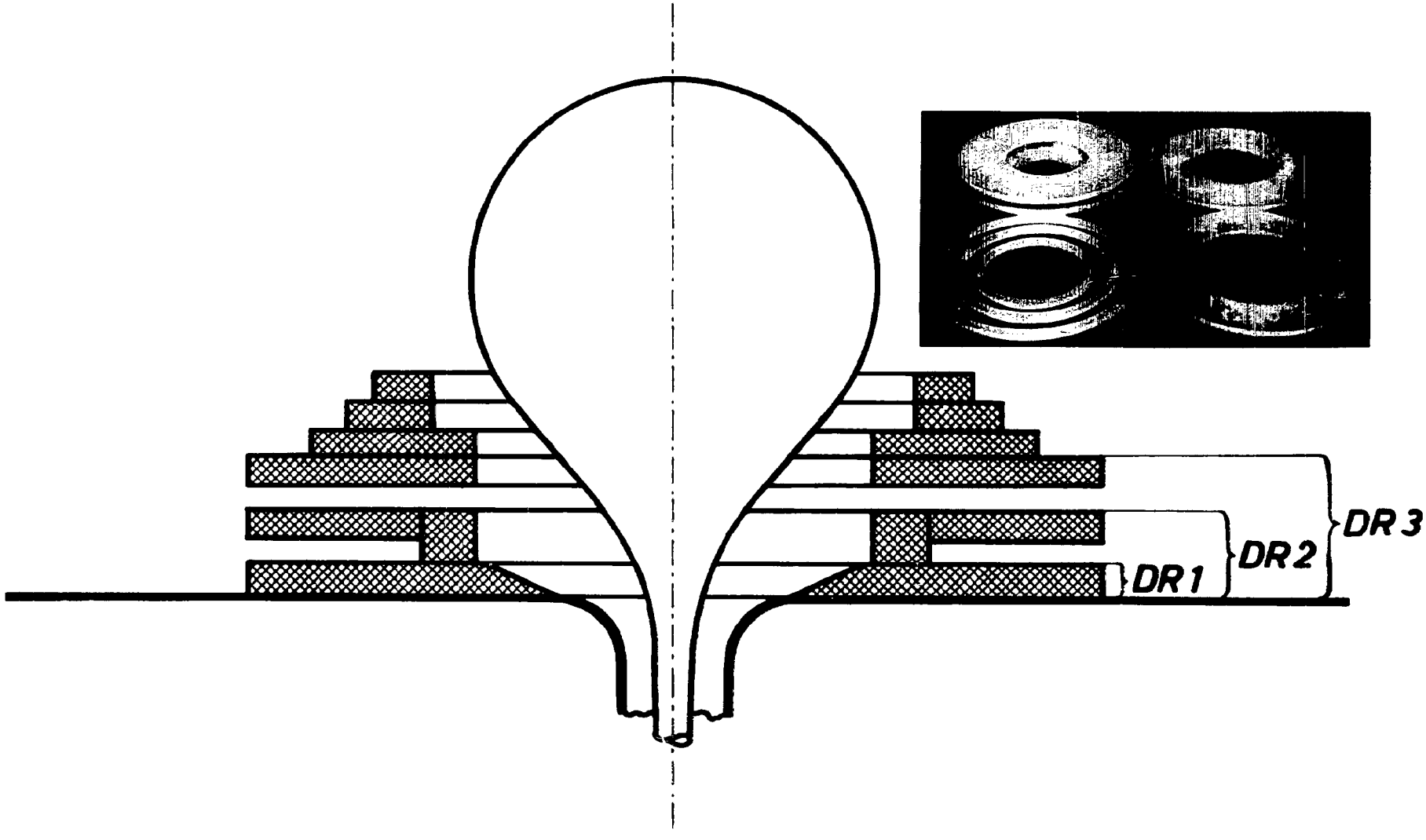

Fig.11

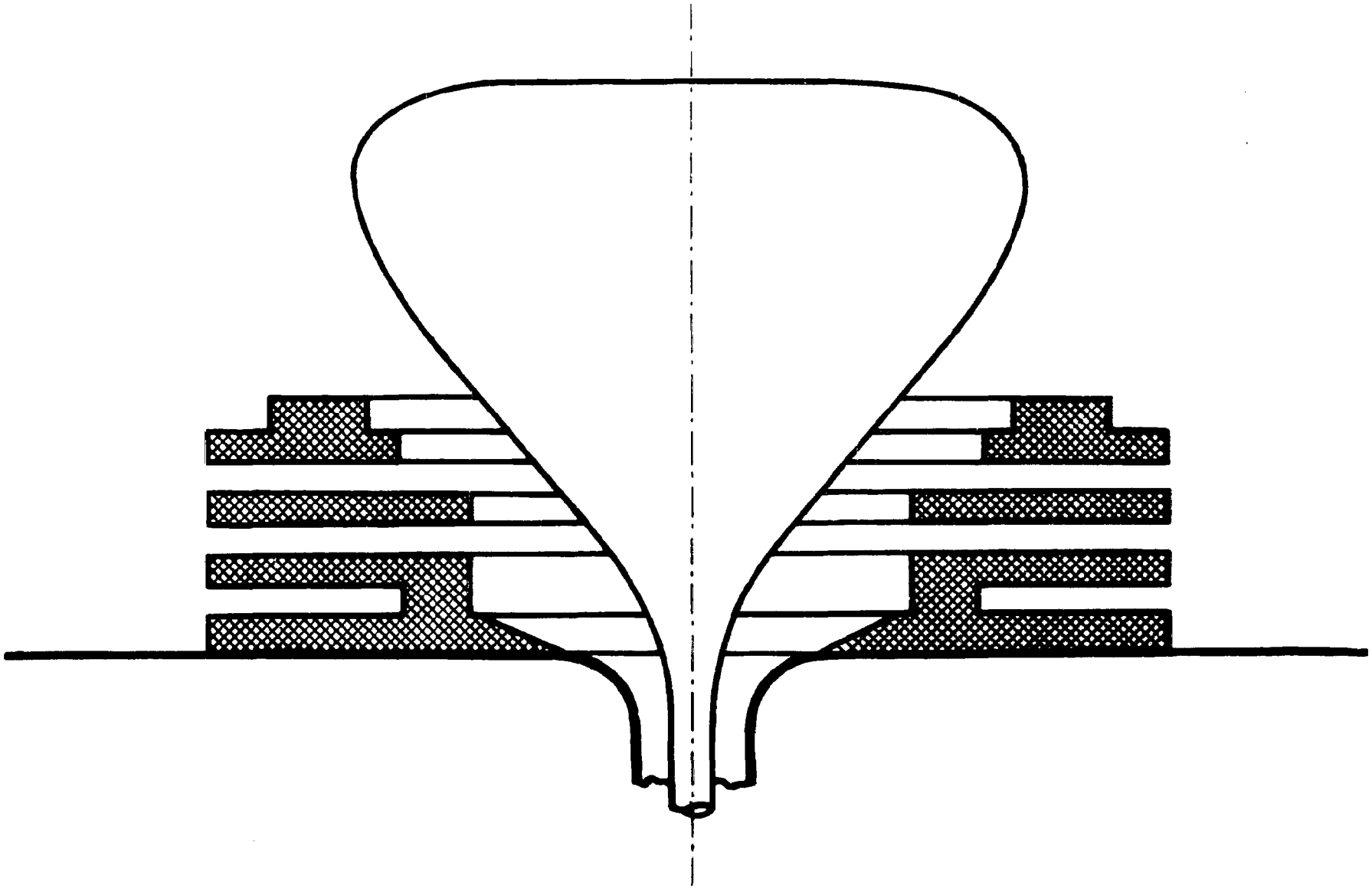

Fig.12

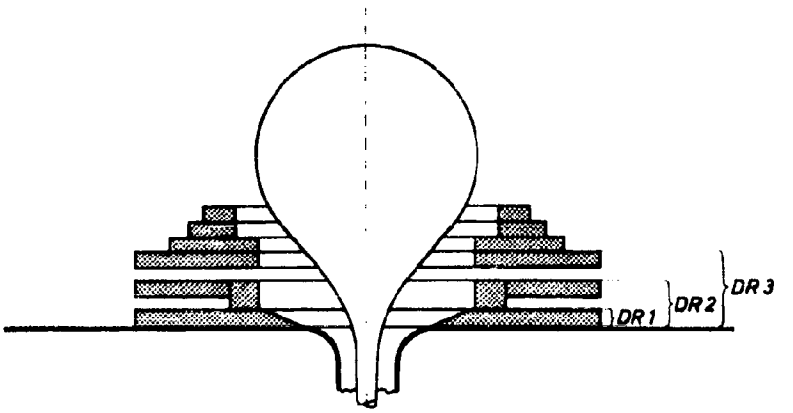

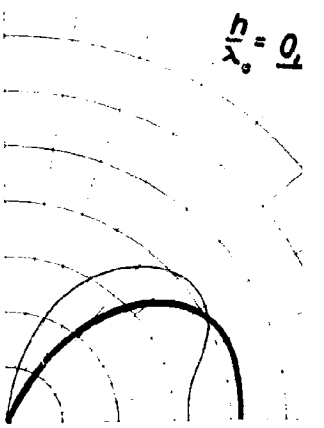

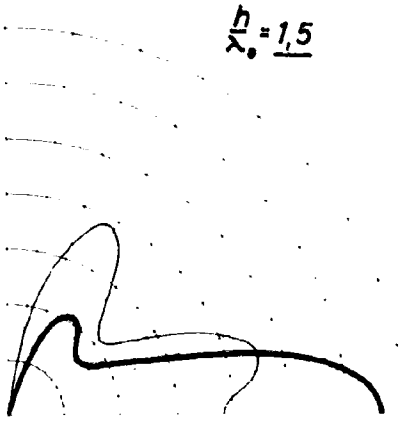

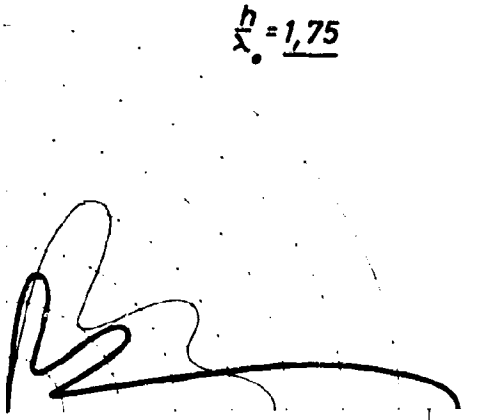

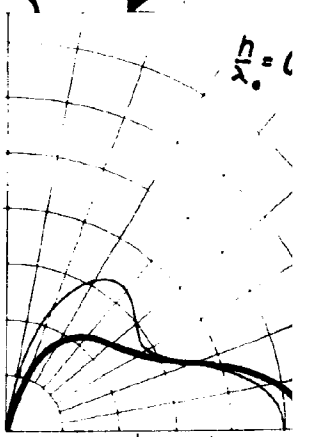

1

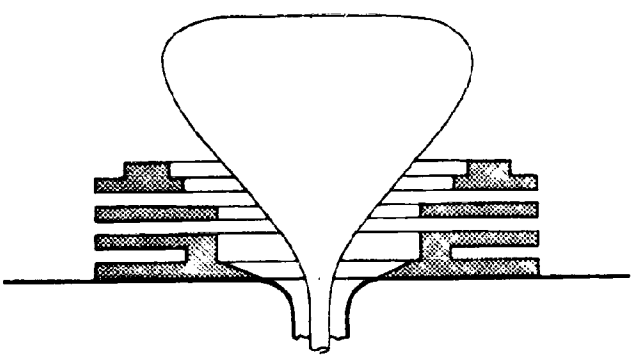

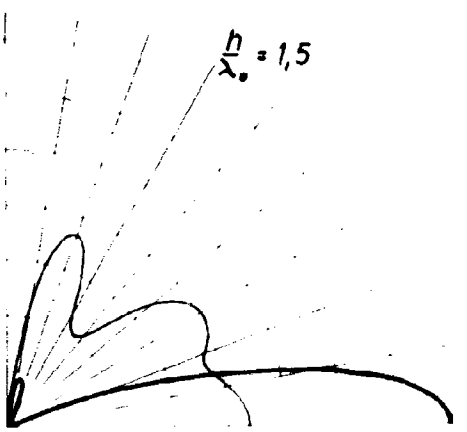

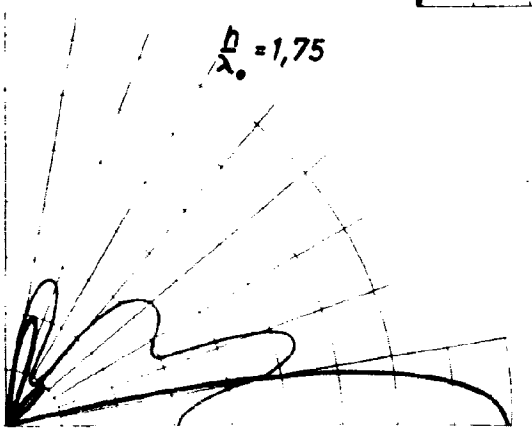

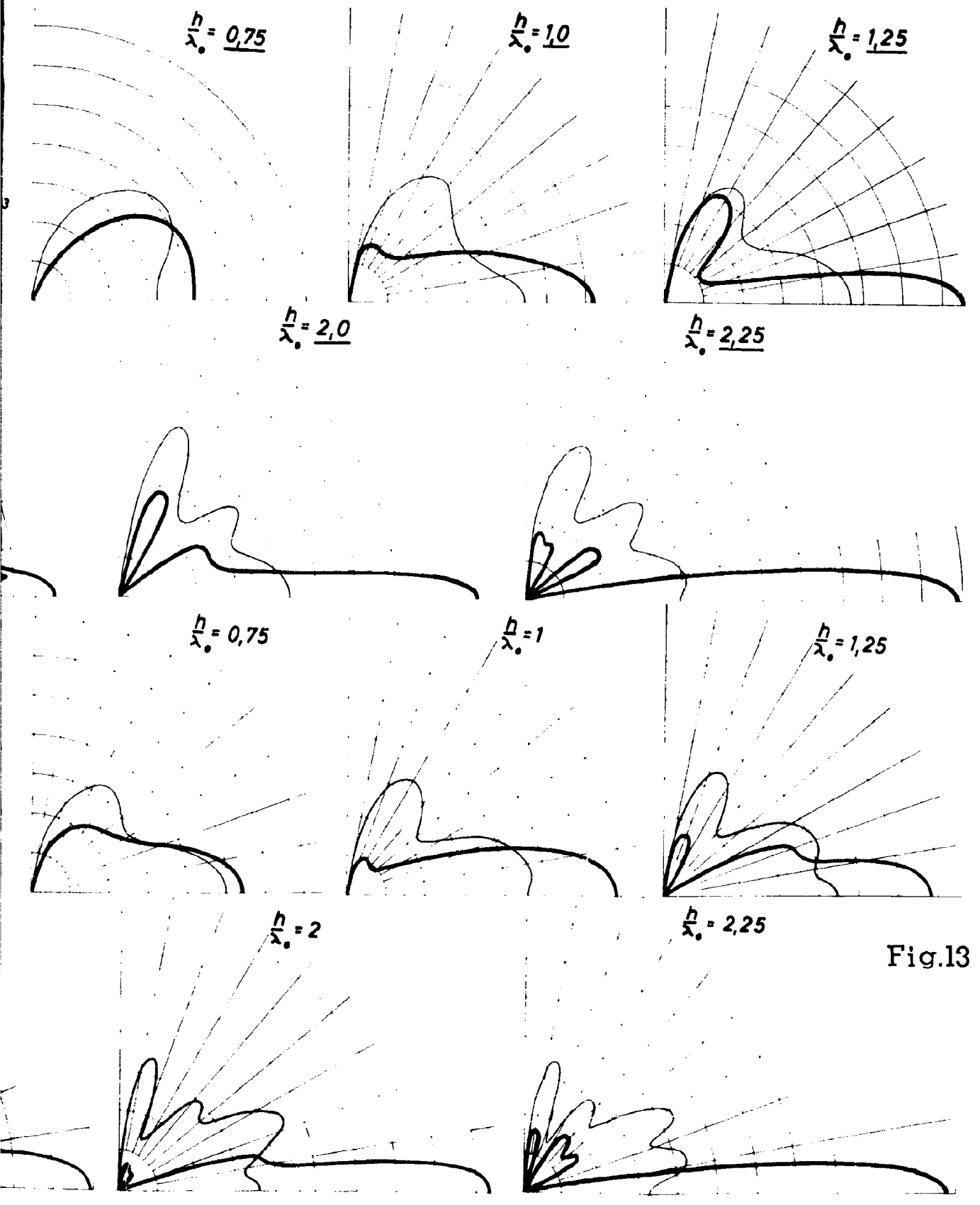
h/λ₀ = 0,75
h/λ₀ = 1,0
h/λ₀ = 1,25
h/λ₀ = 2,0
h/λ₀ = 2,25
h/λ₀ = 0,75
h/λ₀ = 1
h/λ₀ = 1,25
h/λ₀ = 2
h/λ₀ = 2,25

Fig.13

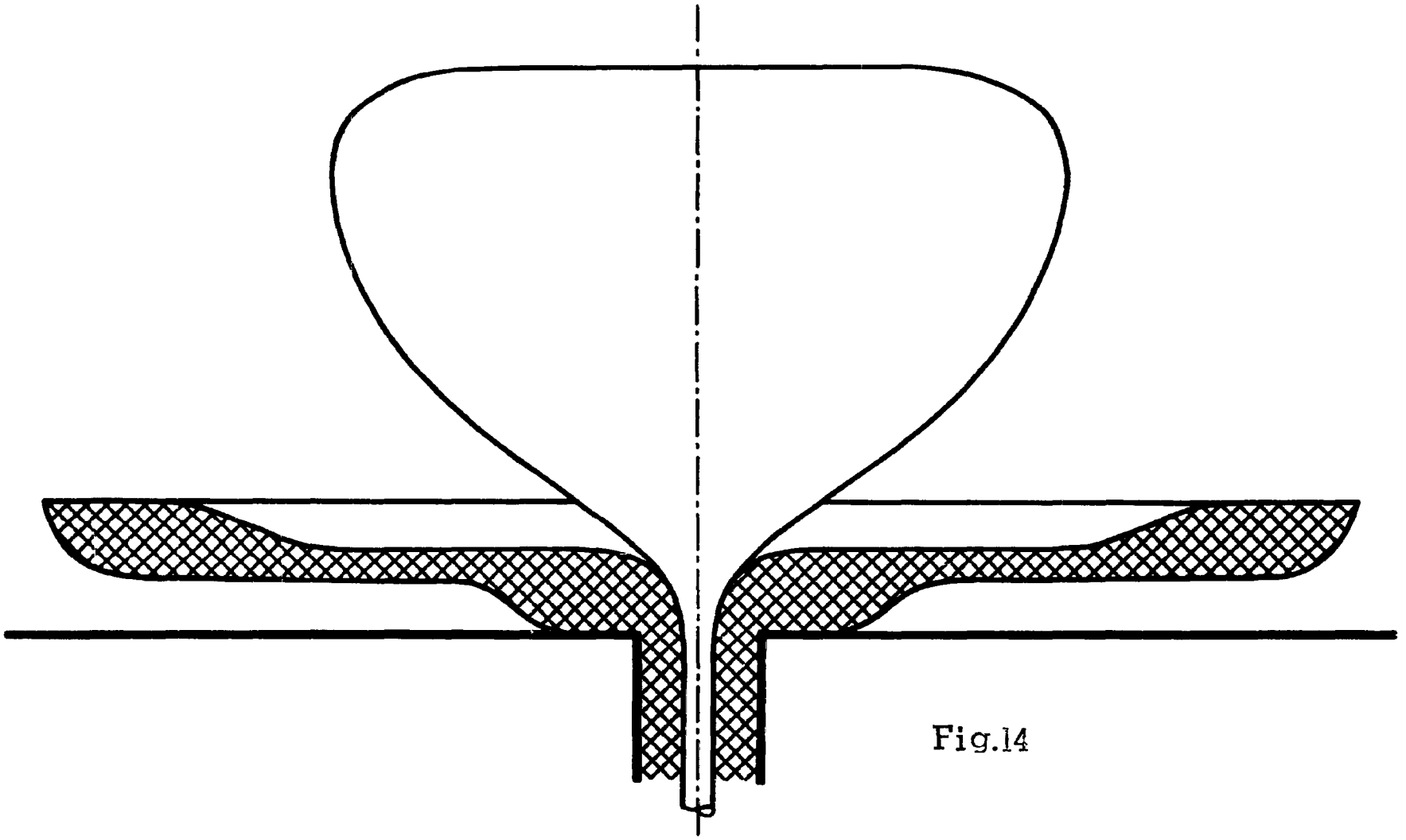

Fig.14

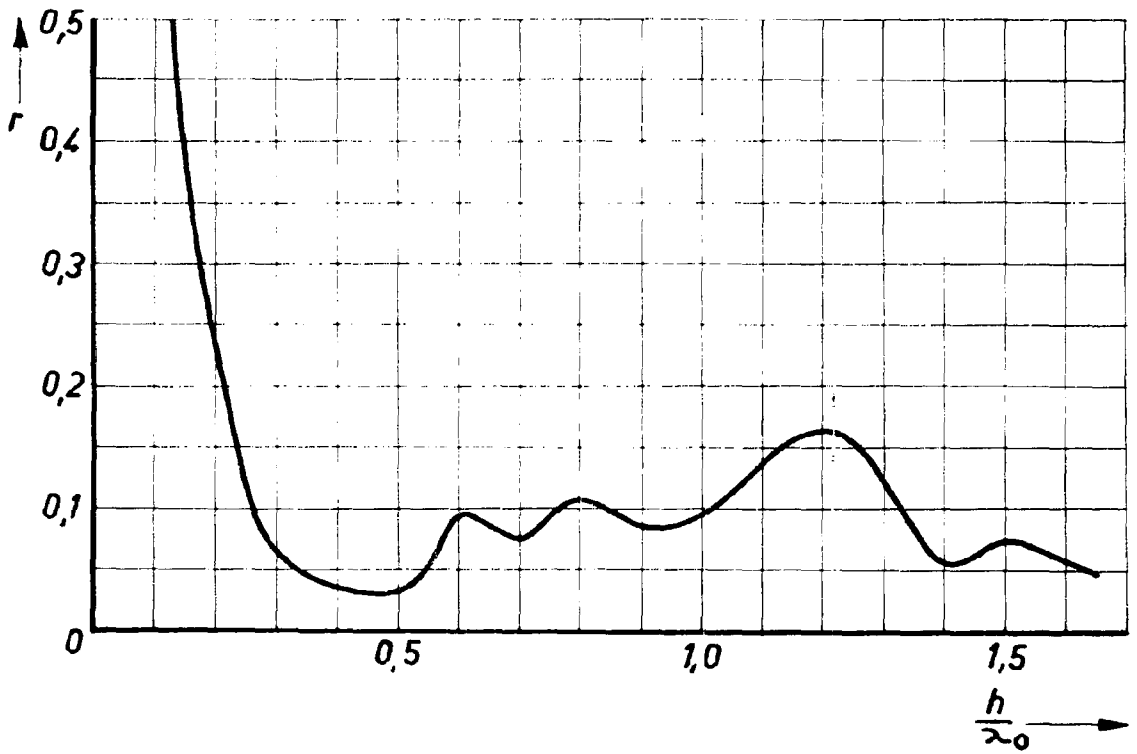

Fig.15

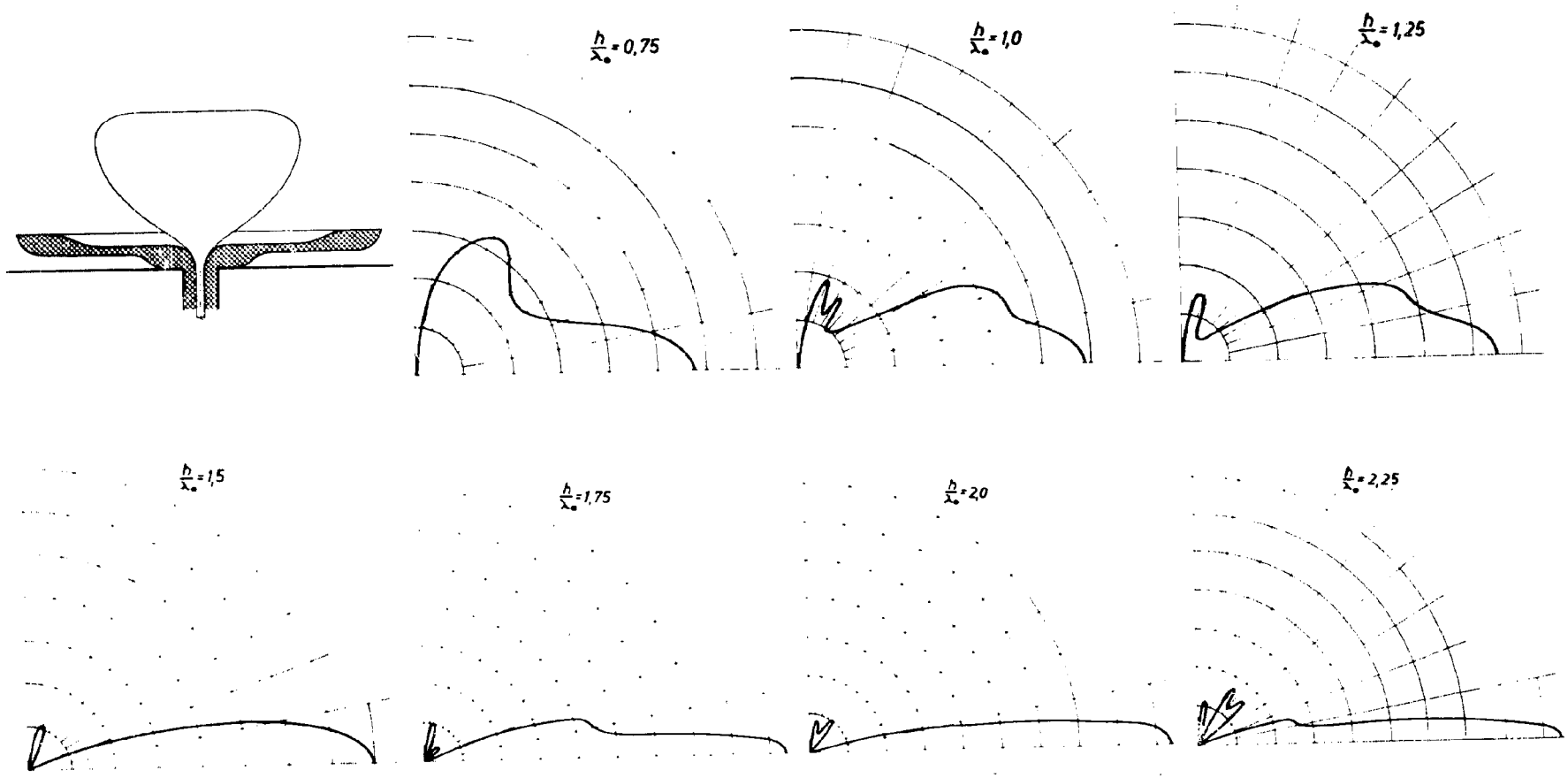

Fig.13

shape in the vicinity of the radiator feeding zone. The reflection factor and the radiation pattern are displayed in Fig. 15 and 16.

Part 3 A Curved Line Coordinate System for Calculating the Radiation Field of a 60 ohm Spherical Radiator

The mathematical treatment of the radiation process of broadband radiators is extremely difficult. Especially, since the formation of the Maxwell equations that describe the radiation field, requires the insertion of the boundary conditions of the field at the edge of the radiator and ground plane, and this is an extremely difficult problem to solve. However, the possibility exists, that one can obtain very simple boundary conditions, if a coordinate system is introduced, in which the ground plane, as well as the radiator itself, are coordinate lines. An orthogonal curved line coordinate system which fulfills these conditions is obtained, for example, from the equipotential lines and field lines of the static field, that exists when a dc voltage is applied between radiator and ground plane. Fig 17 shows the static field of a 60 ohm radiator. The Maxwell equations of the radiation field have been set up in the curved line coordinate system in [5] . Through a suitable insertion which describes the complete field as the sum of complex partial wave functions W_n, the partial differential equations break down into an infinite number of ordinary, 2nd order, coupled differential equations, i.e. the differential equations for W_0 and W_1 yield:

$$\left(\frac{\lambda_0}{2\pi}\right)^2 W_0'' + F_0 W_0 = -\left(\frac{1}{2}F_1 W_1 + \frac{1}{2}F_2 W_2 + \frac{1}{2}F_3 W_3 + \cdots\right) \tag{1}$$

$$\left(\frac{\lambda_0}{2\pi}\right)^2 W_1'' + \left[\left(F_0 + \frac{1}{2}F_2\right) - \left(\frac{\lambda_0}{2a}\right)^2 \left(G_0 - \frac{1}{2}G_2\right)\right] W_1 \tag{2}$$

$$= -\left\{F_1 W_0 + \left[\frac{1}{2}(F_1 + F_3) - \left(\frac{\lambda_0}{2a}\right)^2 (G_1 - G_3)\right] W_2 + \cdots\right\}$$

0
0,5
1,0
1,5
2,0
3,0
2,5
2,0
1
1

Fig.17

The values of F_n and G_n can be obtained with the help of the graphical Fourier analysis from the curved line coordinate system; for the 60 ohm spherical radiator they are shown in [15, Figs. 40 and 41] . The solution of the differential equations by means of electrical computers is now possible in principle. However, this is very difficult to do for antennas of practical importance, since the values F_n and G_n become infinite at the antenna apex. Therefore a coordinate system, in which both the ground plane and the radiating part of the antenna surface are coordinate lines, and also have finite values for F_n and G_n in the apex vicinity, is the most suitable system for our purposes.

However, the equipotential lines, which describe the radiation surface, may not enclose themselves as before, but must peel off in the vicinity of the radiator vertex of the actual antenna shape and continue toward infinity. It is especially advantageous if we could allow this equipotential line to flow into an infinite extension cone (as shown in Fig. 18) the vertex of which lies in the ground plane.

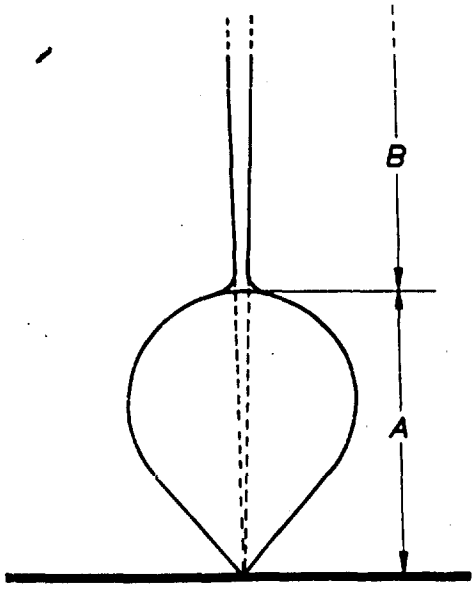

Fig.18

The resulting coordinate system matches the electrostatic field of a conical line, more and more, as the distance from the null increases. F_o takes on a large, but finite value with increasing distance from the origin, while all higher order F_n have zero as their asymptotes. From this we are able to obtain the most suitable boundary conditions for solving the differential equations, this being, that reflected waves no longer exist at a sufficient distance from the origin.

I. Experiments Indicating the Permissability of an Infinite Extension Cone Arrangement

Before we can actually use this coordinate system, it must be shown that the electrical relationships of a broad-band radiator with an infinite extension cone does not depart considerably from the final desired antenna shape. In [4] it can be seen that the shape of the radiation pattern is independent of the antenna length, if the current along the radiator decreases rapidly, as is the case with large radiation attenuation, and the upper current-less regions of the antenna do not contribute anything toward radiation.

Therefore our new coordinate system is only suitable with large radiation attenuation, since this is the only condition which causes the current along the antenna to decrease rapidly and become so small at the antenna crest, such that the addition of an extension cone at the top does not cause a noticeable change in the radiation behaviour.

The boundary field lines of each wave type, W_n progress towards the antenna feeding zone with increasing frequency, such that, the radiation process becomes more concentrated about the lower portion of the antenna. Also it is to be expected, that the impedance and radiation behaviour becomes continuously more independent of the radiator shape in the vicinity of its vertex, as the frequency increases. This can also be confirmed by the experiments described below.

Next, the matching factor "m" (reciprocal SWR):

$$m = \frac{V_{min.}}{V_{max.}}$$

of the 60 ohm spherical radiator was measured by using part of the input line as a slotted line. The results are shown in Fig.19, curve a. If a thin brass rod is added to the top of the antenna vortex, as shown in Fig.20 and "m" is measured again, the results as shown by curve b of Fig.19 are obtained. It can be seen that curve b pendulates about curve a and the amplitudes of these fluctuations become increasingly smaller with increasing frequency. This can be explained in the following manner: The spherical radiator looks like an inhomogeneous line with losses that is terminated with the input impedance of a thin rod antenna.

This rod antenna has the known curve in the complex impedance plane, as a function of increasing frequency, as shown in Fig.21. The periodic variation of the input impedance of the rod antenna causes the measured variations of the matching factor "m" shown in Fig.19 by curve b.

If the attenuation of the inhomogeneous line located between the rod antenna and the slotted line becomes larger; that is, if the radiation attenuation becomes larger in the middle and lower regions of the spherical radiator, then the variations of the input impedance of the rod antenna has a continuously decreasing effect upon the matching factor "m". Since the radiation attenuation increases with increasing frequency, the variation of the matching factor decreases.

A similar effect can be seen, if one measures the radiation pattern of the 60 ohm spherical radiator, first with and then without the rod antenna, and compares the results (Fig.22). The curves "b" pendulate about the curves "a" and the am-

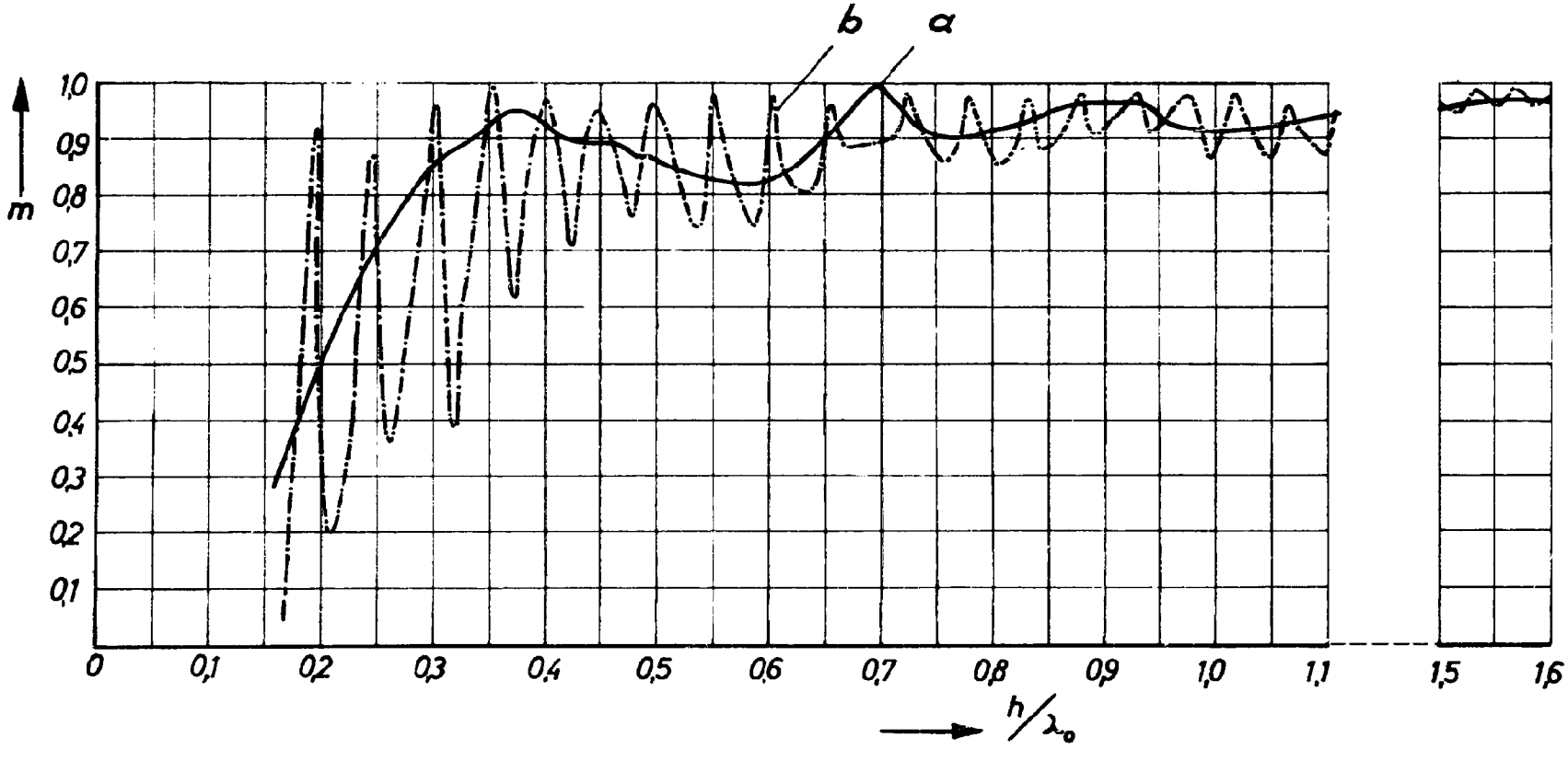
b
a
m
1,0
0,9
0,8
0,7
0,6
0,5
0,4
0,3
0,2
0,1
0
0,1
0,2
0,3
0,4
0,5
0,6
0,7
0,8
0,9
1,0
1,1
1,5
1,6
h/λ₀

Fig.19

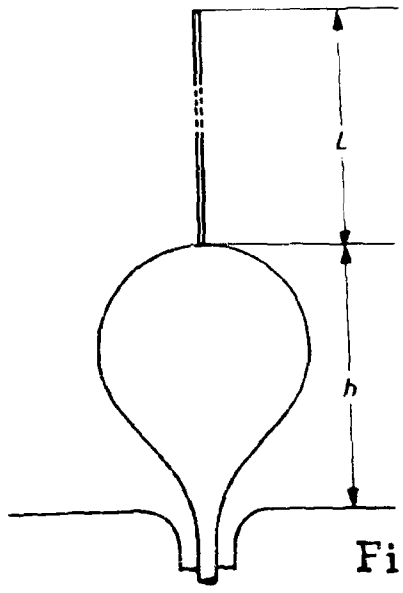

Fig.20

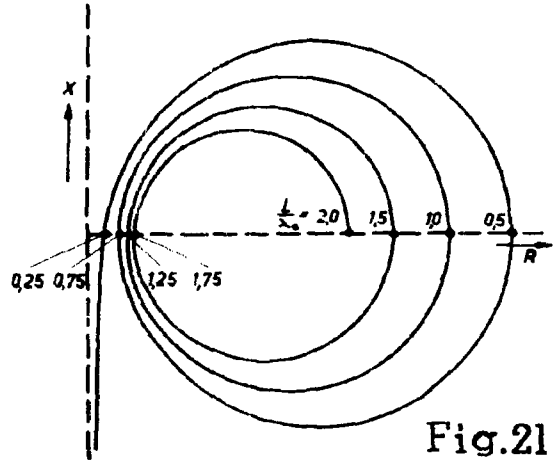

Fig.21

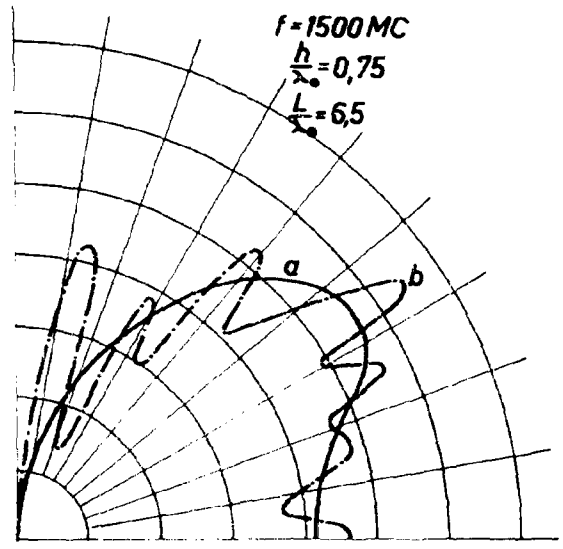

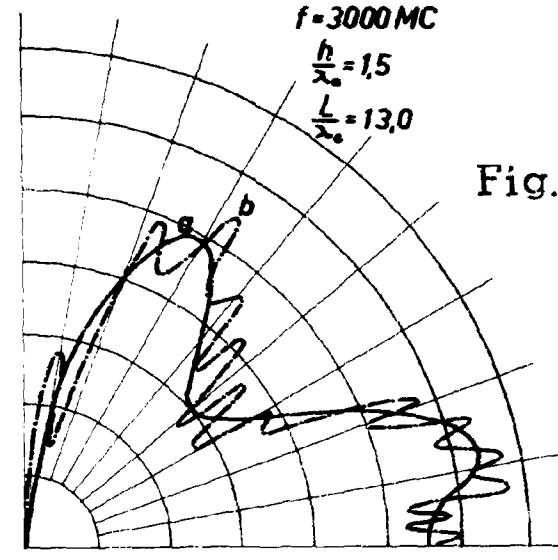

Fig.22

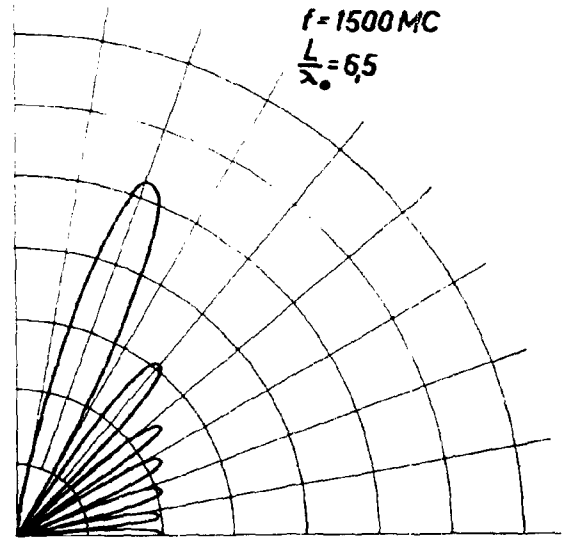

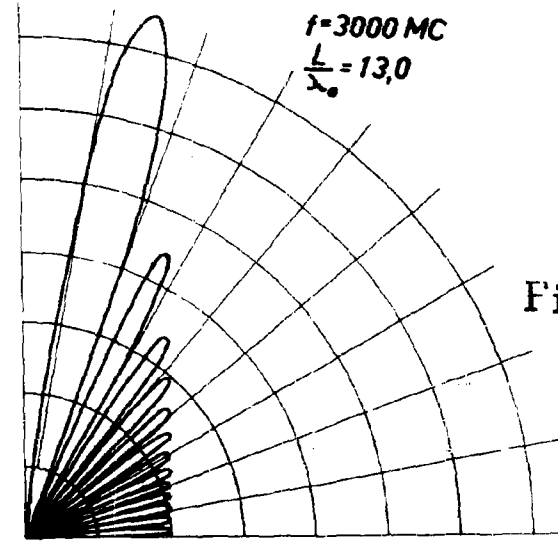

Fig.23

pitude of the deviations is notably smaller at 3 000 mc. than at 1 500 mc. In order to clarify this effect, the radiation patterns of the thin rod antenna of length, L = 130 cm., were calculated for both frequencies of 1 500 mc. and 3 000 mc. according to the familiar equation (3) [reference 16]

$$F_{n;}(\Theta, \beta_o h) = \frac{\cos(\beta_o h \cos\Theta) - \cos \beta_o h}{\sin \Theta} \qquad (3)$$

and drawn in Fig.23. If one compares the curves "b" of Fig.22 with the curves of Fig.23, one can easily see that the number of deviation maxima of the curves "b" in Fig.22 is the same as the number of side lobes in Fig.23 for both frequencies. The pendulation of curve "b" in Fig.22 originates from the radiation pattern of the additional rod antenna, since this pattern now combines with that of the 60 ohm spherical radiator. The decrease in pendulation with increasing frequency proves that the radiation attenuation of the 60Ω radiator increases accordingly, and thus the residual current, at the crest of the spherical radiator and along the rod antenna, becomes continuously smaller. (That the deviation maxima of curves "b" in Fig.22 are not in exact agreement with the side lobes of Fig.23, in respect to their angular positions, is not important in this analysis. This results from the fact that the radiation patterns of Fig.22 were only measured at a relatively short distance, $R \approx 2L$, from the feeding point, whereas the equation (3) is only exact for the distant field.)

As expected, the impedance and radiation behavior, becomes increasingly more independant of the antenna shape in the vicinity of its apex, as the frequency is increased. Therefore it has been proven sufficiently, that the use of a coordinate system with an infinite extension cone is satisfactory at higher frequencies.

II. The Calculation by means of Line Charges, of a Coordinate System with an Infinite Extension Cone

All the coordinate systems that we have previously used, were calculated from suitably chosen charge distributions, along the radiator axis since this criterion enables us to avoid the boundary problem of the potential equation.

An infinitesimally small line charge, has the potential of a point charge.

$$\phi_c = \frac{q(h_o)\, dh_o}{4\pi\varepsilon_o R} \tag{4}$$

In accordance with Figure 7a

$q(h_o)$ is the charge density;

h_o is the position of the line element dh_o on the radiator axis;

$R = \sqrt{r^2 + (h - h_o)^2}$ is the distance of the point P(r,h) from this line charge element.

By inserting the equation for R and integrating from $-\infty$ to $+\infty$, the resulting equation for ϕ at P(r,h) becomes:

$$\phi = \frac{1}{4\pi\varepsilon_o} \int_{-\infty}^{+\infty} \frac{q(h_o)\, dh_o}{\sqrt{(h-h_o)^2 + r^2}} \tag{5}$$

The condition that the ground plane, which corresponds to $h = 0$, always be an equipotential surface having the potential $\phi = 0$, can be fulfilled if the following relationship of the function $q(h_o)$ is forced to hold true:

$$q(-h_o) = -q(h_o) \tag{6}$$

One can achieve this condition that the radiator surface, which is symmetrical upon rotation about its axis, be an equipotential

surface, if further stipulations are applied to the function $q(h_c)$.

The integral (7) is only completely solvable for a few line distribution functions $q(h_o)$. However the charge distribution of all radiator shapes having a finite height, is limited to a finite region of the radiator axis, and therefore the following is true:

$$q'(h_o) \begin{cases} \neq 0 & \text{for } -a < h_o < a \\ = 0 & \text{for } -a > h_o > a \end{cases} \qquad (7)$$

Fig.25 shows the charge distribution for the 60 ohm spherical radiator. In this case, numerical solutions of the integration can be accomplished with the aid of an electronic computer, if one substitutes a step polygon for the function $q(h_o)$ as shown in Fig.26. In addition, the distance "2a" is divided into N intervals, each of which is Δh_o long and the heights of the resulting rectangles are made to be the ordinate of the curve in the middle of the interval (tangential method). The potential of the line charge in point P(r h) can be calculated as a finite sum, in accordance with the following equation (8).

$$\Phi = \frac{\Delta h_o}{4\pi\varepsilon_o} \sum_{n=1}^{N} \frac{q_n}{\sqrt{(h-h_{on})^2 + r^2}} \qquad (8)$$

However if the equipotential surface which describes the radiator surface area, peels off the actual antenna shape in the vicinity of the antenna vertex, and it be required to extend into an infinite extension cone, then the corresponding charge distribution must also extend to infinity along the radiator axis.

Therefore, a numerical calculation of the potential, using the tangential method, is impossible for this particular case.

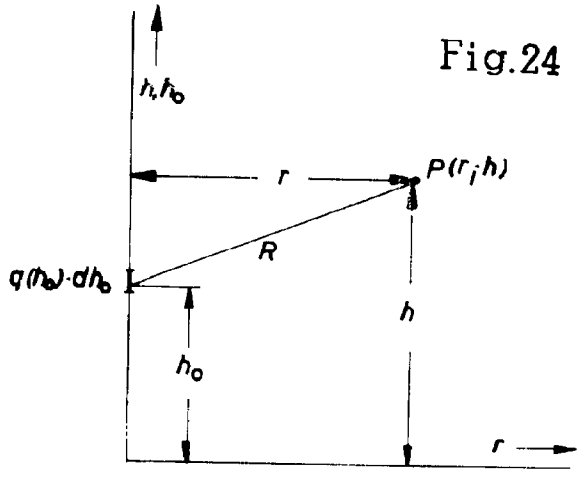

Fig.24

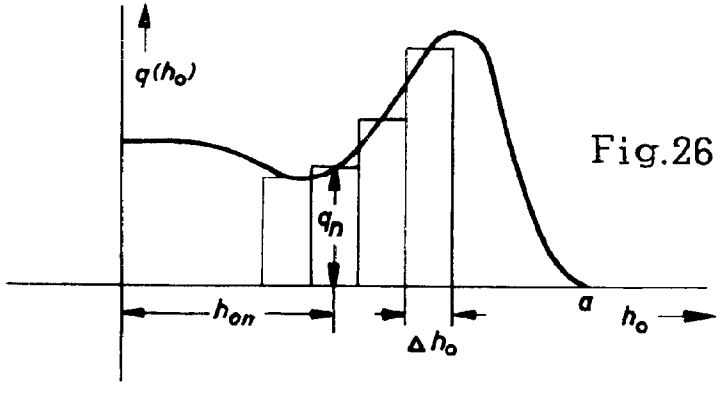

Fig.26

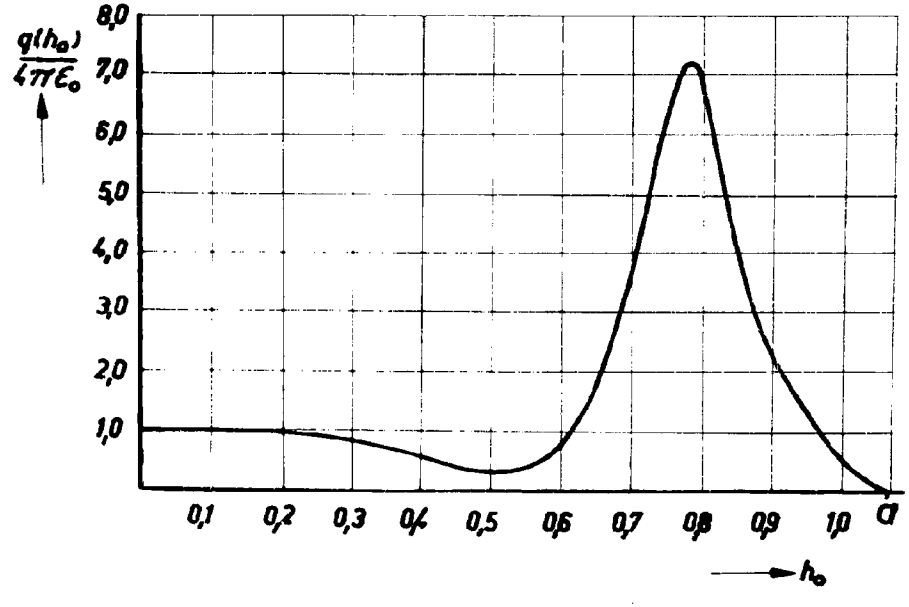

Fig.25

since the integral (5) can now only be written as the sum of an infinite number of terms. Therefore, the charge distribution is always divided into two parts. The first part $q_1(h_o)$, is limited to the region along the radiator axis difined by $-a \leq h_o \leq +a$, and is now usable in (8). The second part $q_2(h_o)$, originates from a suitable line distribution function extended from $-b$ to $+\infty$ for which the integral (5) is solvable in closed form.

II,7) Some Special Distribution Functions $q_2(h_o)$

The simplest procedure assuring the running out of the potential surface into the infinite extension cone, requires the retainment of the part $q_1(h_o)$ as the charge distribution for the finite radiator shape, and taking a distribution function according to (9) and Fig.27 as the second part $q_2(h_o)$.

$$q_2(h_o) = \begin{cases} q_o & \text{for} \quad 0 \leq h_o \leq \infty \\ -q_o & \text{for} \quad -\infty \leq h_o \leq 0 \end{cases} \tag{9}$$

The equipotential surfaces of these line charge $q_2(h_o)$ are infinitely high, cones of revolution about the radiator axis all having the same cone vertex in the zero point (Fig.28). The potential ϕ_2 on a cone surface with the half aperture angle Θ, is directly proportional to the density of the charge distribution according to the following equation: (10a) [reference 15]

$$\phi_2 = \frac{q_o}{2\pi\varepsilon_o} \ln \cot \frac{\Theta}{2} \tag{10a}$$

The above equation can also be written in the following form: (10b)

$$\cot\Theta = \sinh \frac{2\pi\varepsilon_o \phi_2}{q_o} \tag{10b}$$

The value of q_o is determined by (10a) & (10b) if one assumes the aperture angle, $2\Theta_o$ of the extension cone, and requires

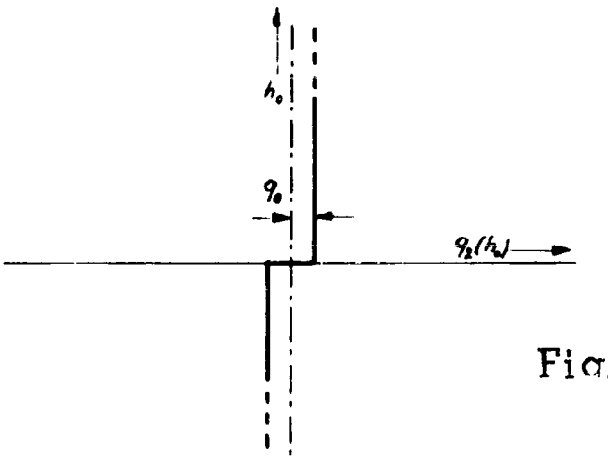

Fig. 27

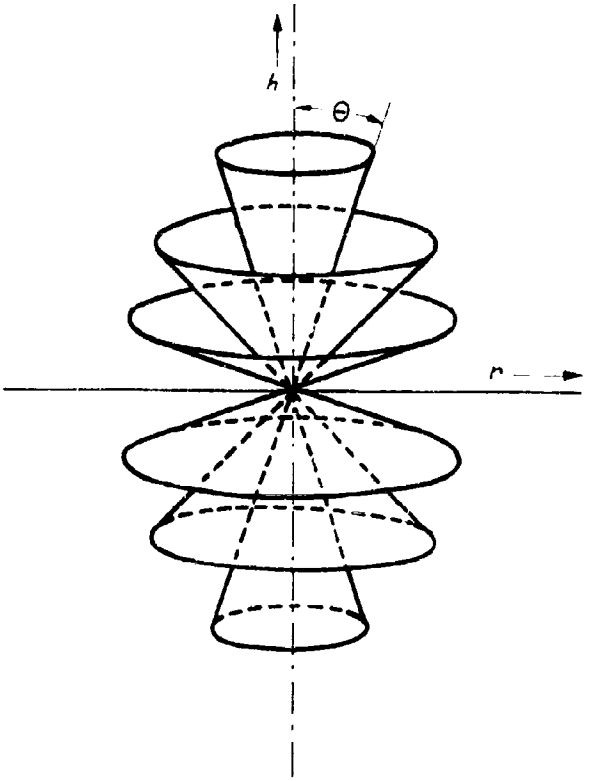

Fig. 28

that the line charge $q_2(h_o)$ causes a potential ϕ_2^* on the surface of this extension cone. This potential ϕ_2^* must be equal to ϕ_1^* which is determined by the charge distribution $q_1(h_o)$ on the surface of the finite radiator shape. Since the charge distribution $q_1(h_o)$ is limited to the region $-a \leq h_o \leq a$ of the radiator axis, the total potential $\phi = \phi_1 + \phi_2$ is determined more and more by ϕ_1 and less by ϕ_2 as the distance form the zero point is increased, such that all potential surfaces, ϕ = constant, converge about the surfaces of the cones where ϕ_2 = constant, as the distance from the origin of the coordinates is increased. Conversely, the potential $\phi = \phi_1 + \phi_2$ must be almost completely determined by ϕ_1 in the vicinity of that part of the radiator surface indicated by A in Fig. 18 (that means $\phi_2 \ll \phi_1$) such that this part of the radiator surface can be described accurately enough by a potential surface ϕ = constant. The condition $\phi_2 \ll \phi_1$ is only fulfilled if the density q_o of the line charge $q_2(h_o)$ is very small, which again has the same meaning, in accordance with (10), as the requirement of a very small aperture angle $2\vartheta_o$ of the extension cone.

A charge distribution which was first calculated for the finite antenna shape, only yields a useful coordinate system when it is combined with a line charge in accordance with (9) and Fig. 17 if one assumes an extremely small aperture angle $2\vartheta_o$.

However the choice of a too small aperture angle is not to be recommended in practice since the equipotential surfaces will then be so intensely concentrated around the extension cone that they can no longer be plotted with the necessary accuracy. In addition, the boundary value $F_o(\infty)$, which the characteristic value F_o approaches with increasing distance from the zero points must not become too large in accordance with the previously mentioned reasons at the beginning of part 3. This also means that ϑ_o may not be made too small since $F_o(\infty)$

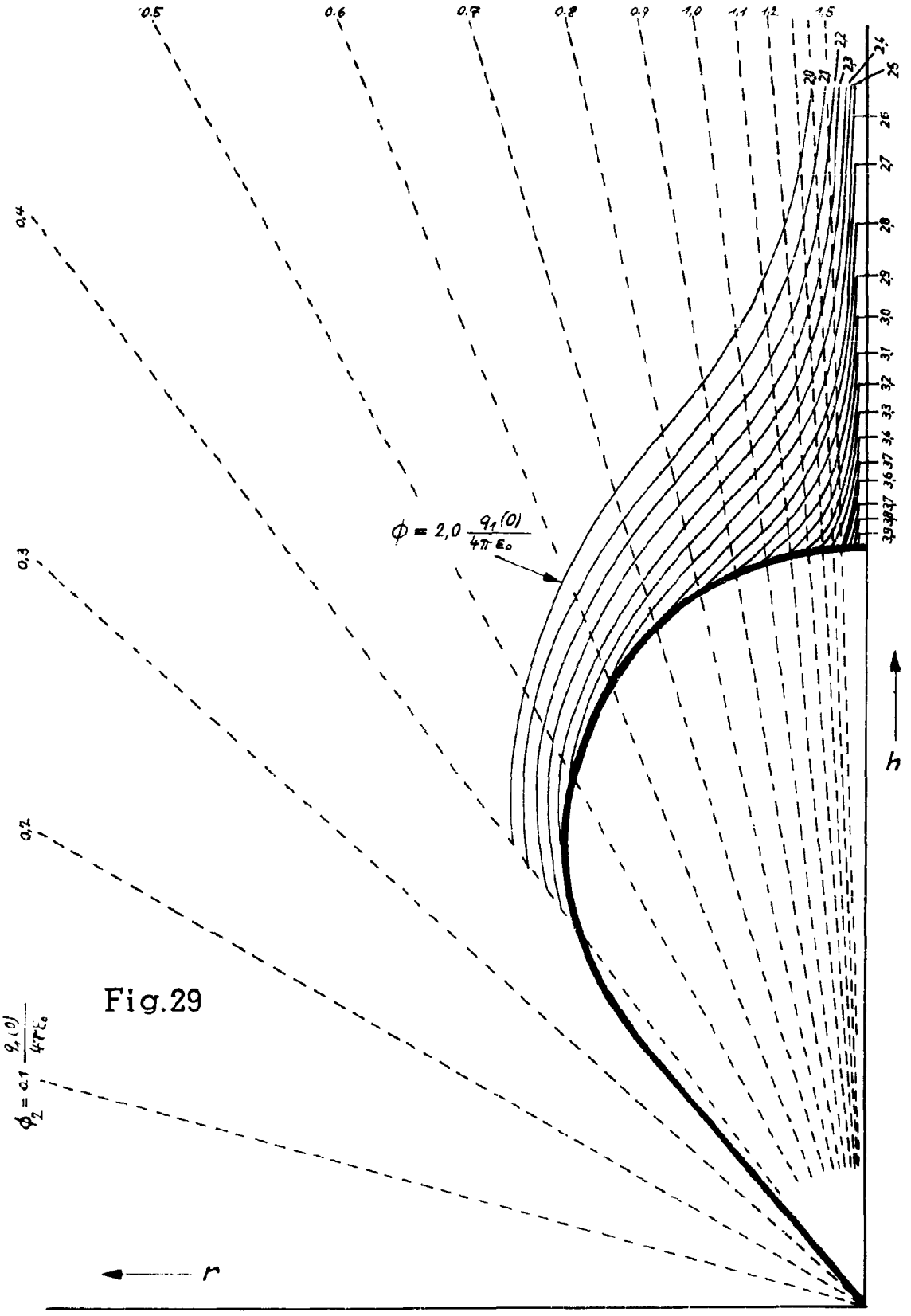
0.5
0.6
0.7
0.8
0.9
1.0
1.1
1.2
1.5
0.4
0.3
0.2
$\phi = 2{,}0\ \frac{q_1(0)}{4\pi\varepsilon_0}$
$\phi_2 = 0.1\ \frac{q_1(0)}{4\pi\varepsilon_0}$
h
r

Fig.29

and Θ_0 are dependent upon each other in the manner shown in equation (11) [reference 5].

$$F_0(\infty) = K \left(\ln \cot \frac{\Theta_0}{2}\right)^2 \qquad (11)$$

K = constant

These considerations indicate that a lower limit of 1° for the aperture angle is appropriate.

Now it should be investigated if the proceedures described yield useful results for an aperture angle $2\Theta_0 = 1°$. This investigation is quickly accomplished for the 60 ohm spherical radiator since the charge distribution $q_1(h_0)$ of the finite radiator sphere (Fig.25) and the potential lines Φ_1 = constant (Fig.27) are well known. The combination of the line charge $q_2(h_0)$ according to (9) and Fig.27 can be simply accomplished by inserting into Fig.27 the lines obtained from equation (10) (that means the meridian sections of the equipotential cones Φ_2 = constant) and joining all the intersections having the same potential $\Phi = \Phi_1 + \Phi_2$.

The surface of the 60 ohm spherical radiator is described by the potential line lying furthermost to the right. There the charge distribution $q_1 h_0$ in accordance with [reference 15] causes a potential value:

$$\Phi_1^* = 2,0 \frac{q_1(h)}{4\pi\varepsilon_0} \qquad (12)$$

Therefore h_0 must be defined in such a way that the line charge $q_2(h_0)$ develops the same value of potential on the surface of the cone with an aperture angle $2\Theta_0 = 1°$.

$$\Phi_2^* = 2,0 \frac{q_2(h)}{4\pi\varepsilon_0}$$

This results in:

$$h_0 = 0,4814 \cdot q_1(0) \qquad (13)$$

The meridian bisections of the corresponding equipotential cones ϕ_2 = constant has been indicated in Fig 29 with dashed lines. If one combines these with the potential lines ϕ_1 = constant in Fig.17 then one obtains the potential lines $\phi = \phi_1 + \phi_2$ = constant, as shown in Fig.29.

The choice of q_o in (13) guarantees that the potential line

$$\phi = 2\pi \frac{q_1(o)}{4\pi\varepsilon_o}$$

converges against the required extension cone having a 1° aperture angle, as the distance from the zero point is increased; thus the desired closeness of these potential line to the shape of the 50 ohm spherical radiator shown by the thick lines in Fig. 29 was not actually obtained.

Thus it can be seen that the intensity q_1 of the line charge $q_2(h_o)$ is already too large if one chooses an aperture angle of the extension cone of $2\Theta_o = 1°$. Therefore a simple combination of this line charge $q_2(h_o)$ with the originally calculated charge distribution $q_1(h_o)$ of the finite radiator shape no longer gives a usable coordinate system.

It can be approximated that the described process yields a potential surface ϕ = constant which hugs the radiator surface well enough in the region A of Fig. 8 and runs out in the region B into the previously described extension cone of aperture angle $2\Theta_o$, if values under 0.5 seconds are inserted for $2\Theta_o$.

However, the disturbing influence of the line charge $q_2(h_o)$ upon the region "A" of Fig. 8 can be reduced in a relatively simple manner by superimposing a constant line charge of the same density q_o, extending to $+\infty$, but now one should not allow this line charge to begin in the zero point; rather, the line charge should be allowed to first begin, at a distance h_o from the ground plane. This gives a distribution function $q_2(h_o)$ in accordance with (14) and Fig.30

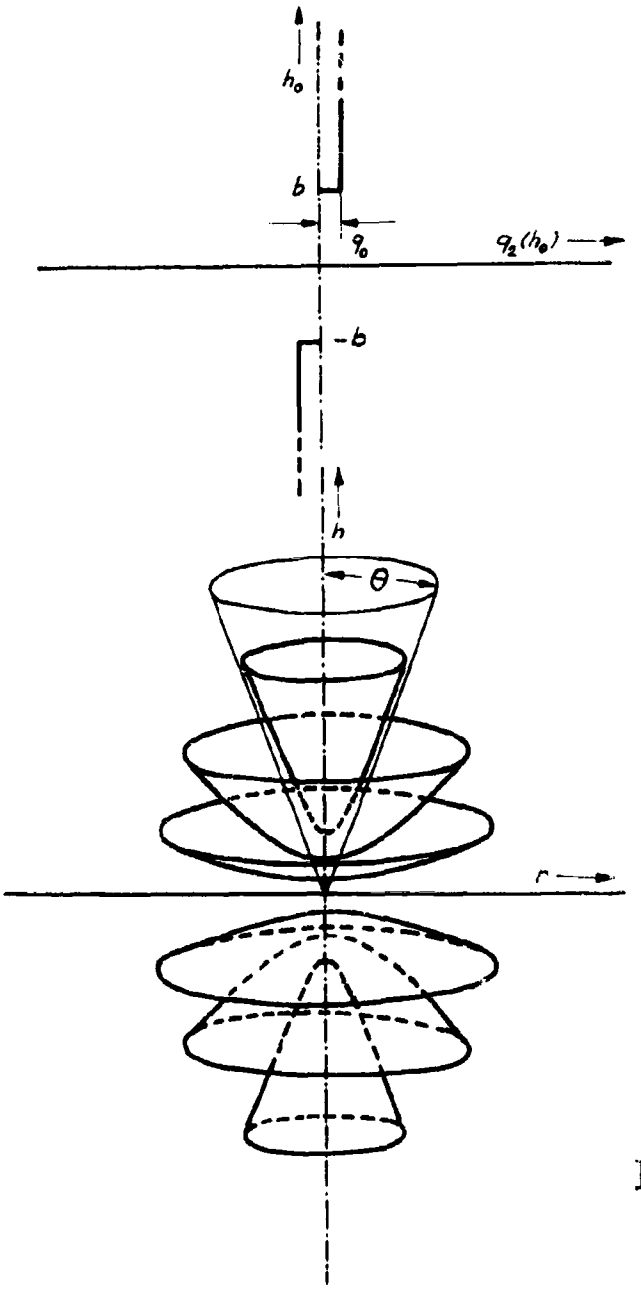

Fig.30

Fig.31

$$q_2(h_o) = \begin{cases} q_o & \text{for } b \leq h_o \leq \infty \\ 0 & \text{for } -b \leq h_o \leq b \\ -q_o & \text{for } -\infty \leq h_o \leq -b \end{cases} \tag{14}$$

The corresponding equipotential surfaces can also be given in explicit form, as is shown in the following. In the above mentioned case, the integral (5) has the following form:

$$\Phi = \frac{q_o}{4\pi\varepsilon_o} \int_b^\infty \left(\frac{1}{\sqrt{r^2 + (h-h_o)^2}} - \frac{1}{\sqrt{r^2 + (h+h_o)^2}} \right) dh_o \tag{15}$$

This integral is solvable if an appropriate substition is made. One then obtains the following equation:

$$\Phi = \frac{q_o}{4\pi\varepsilon_o} \ln \left[\frac{-h + h_o + \sqrt{r^2 + (h-h_o)^2}}{h + h_o + \sqrt{r^2 + (h+h_o)^2}} \right]_b^\infty \tag{16}$$

As h_o approaches infinity, the argument of the natural logarithm term becomes 1, such that the upper boundary in (16) does not contribute anything to Φ. Therefore one obtains

$$\Phi = -\frac{q_o}{4\pi\varepsilon_o} \ln \frac{-h + b + \sqrt{r^2 + (h-b)^2}}{h + b + \sqrt{r^2 + (h+b)^2}} \tag{17}$$

or in the antilogarithmic form:

$$e^{-\frac{4\pi\varepsilon_o \Phi}{q_o}} = \frac{-h + b + \sqrt{r^2 + (h-b)^2}}{h + b + \sqrt{r^2 + (h+b)^2}} \tag{18}$$

One obtains the equation of the equipotential surfaces if one equates:

$$e^{-\frac{4\pi\varepsilon_0\Phi}{q_0}} = \text{const} = C. \tag{19}$$

If one now manipulates the equation somewhat, the following result is obtained: (20)

$$-\frac{r^2}{\frac{4b^2C}{(C+1)^2}} + \frac{h^2}{\frac{b^2(C-1)^2}{(C+1)^2}} = 1 \tag{20}$$

The equipotential surfaces of a line charge according to (14) and Fig.30 are therefore confocal hyperboloids of rotation having two sheets, with the charges line r = 0 as their axis of rotation (Fig.31). The two semi-axes are:

$$a^* = \frac{2b\sqrt{C}}{C+1} \qquad b^* = \frac{b(C-1)}{C+1} \tag{21}$$

The focal points are located at r = 0; h = $\pm$b. Therefore the focal points are those points of the axes according to Fig.30, at which the constant charge distribution q_0 begins. These hyperboloids of revolution converge against the asymtotic cone with the half aperture angle Θ as the distance from the zero point increases

$$\cot\Theta = \frac{b^*}{a^*} = \sinh\frac{2\pi\varepsilon_0\Phi_2}{q_0} \tag{22}$$

A comparison of (22) with (10b) shows that these asymtotic cones are identical to the equipotential cones (Fig.27) of the line charge $q_2(h_0)$ according to (9) and Fig.27. The potential field of the 60 ohm spherical radiator should now be combined with the equipotential surfaces of the line charge $q_2(h_0)$ according to (14) and Fig.30. This can be most easily accomplished by drawing the hyperbolas of equation (20) (that is, the meridian bisections of the hyperboloids of revolution, ϕ_2 = constant) upon Fig.17 and joining all the intersections having the same potential, $\phi = \phi_1 + \phi_2$. The potential lines ϕ = constant which have been achieved in this manner, can be seen in Fig.32; the given hyperboloids, ϕ_2 = constant are also shown by dahed lines in the same figure.

The determination, according to equation (13), of the charge density q_0, guaranties that the potential surface

$$\Phi = \Phi_1 + \Phi_2 = 2{,}0 \frac{q_1(0)}{4\pi\varepsilon_0}$$

runs out into an extension cone with the previously determined aperture angle, 2Θ [illegible] the potential surface conforms much more [illegible] the shape of the 60 ohm spherical radiator (shown with [illegible] lines in Fig.32) than the potential surface with the same [illegible] Fig.29. On the basis of experimental results [illegible] with the wide band antenna project, we can predict, with considerable assurance, that a conducting body of revolution whose shape as defined by the potential line

$$\Phi = 2{,}0 \frac{q_1(0)}{4\pi\varepsilon_0}$$

has the desired characteristics of a broad-band antenna and can hardly be differentiated from the 60 ohm spherical radiator with an infinite extension cone, in respect to its impedance and radiation behaviour.

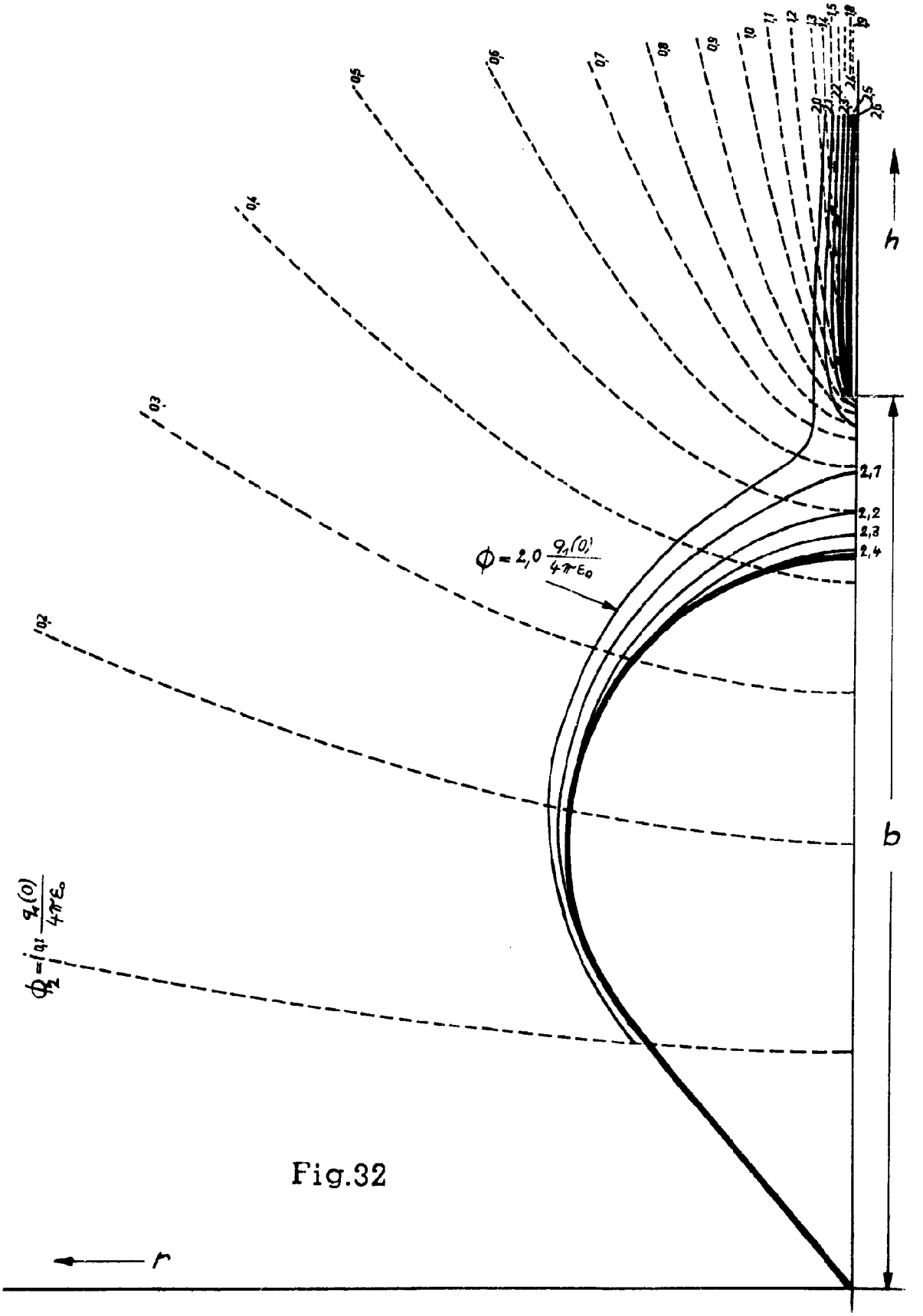
0,2
0,3
0,4
0,5
0,6
0,7
0,8
0,9
1,0
1,1
1,2
1,3
1,4
1,5
1,6
2,1
2,2
2,3
2,4
h
b
r
$\Phi = 2{,}0\,\frac{q_1(0)}{4\pi\varepsilon_0}$
$\Phi_2 = i_{q1}\,\frac{q_1(0)}{4\pi\varepsilon_0}$

Fig.32

II.2 The Distribution Functions $q_1(h_o)$ and $q_2(h_o)$ for the 60 ohm Spherical Radiator with an Infinite Extension Cone having a 1^o Aperture Angle

A charge distribution $q_1(h_o) + q_2(h_o)$ is sought whose equipotential surface

$$\Phi = \Phi_1 + \Phi_2 = 2{,}0 \frac{Q_1(0)}{4\pi\varepsilon_o}$$

describes the surface of the 60 ohm spherical Radiator (in accordance with Fig. 18) in an ideal manner in region "A" and runs out as quickly as possible into the prescribed extension cone of aperture angle $2\vartheta = 1^o$ in such a way that the transition from the radiator vertex in region "B" is fast but without sharp edges.

II.2.1 The Charge Distribution Function $q_2(h_o)$

The integral (9) in closed form must again be solvable for the line charges $q_2(h_o)$ beginning at a distance $\pm b$ from the ground plane and extending to $\pm \infty$.

In Fig. 29 and also Fig. 32, the potential lines

$$\Phi = 2{,}0 \frac{Q_1(0)}{4\pi\varepsilon_o}$$

have the disvatage that they converge much too slowly against the prexcribed extension cone of 1^o aperture angle as the distance h_o from the ground plane is increased. This is caused by the relatively slow decrease of the influence of Φ_1 upon the charge distribution $q_1(h_o)$ (limited to the region $-a \leq h_o \leq a$) as h_o is increased. The distinct quick approaching of the potential line

$$\Phi = 2{,}0 \frac{Q_1(0)}{4\pi\varepsilon_o}$$

to the extension cone, can be obtained however, when one does not assume a constant charge distribution on the radiator axis as indicated in Fig. 27 and Fig. 28, but instead one should allow

the charge density $q_2(h_0)$ to increase as the distance h_0 from the ground plane is increased. An analytically simple distribution funktion $q_2(h_0)$, which increases in the correct manner with h_0, is indicated in the following.

However, the lines having the same part potential ϕ_1 coincide somewhat accurately in region "B" of Fig.18 with the equipotential lines of double point charges $\pm Q_0$ which one can consider as being located at a distance $\pm c$ from the ground plane on the radiator axis. Therefore in region "B" of Fig.18 the following is true:

$$\Phi_1 \approx \frac{Q_0}{4\pi\varepsilon_0}\left(\frac{1}{\sqrt{r^2+(h-c)^2}} - \frac{1}{\sqrt{r^2+(h+c)^2}}\right) \quad (23)$$

Q_0 and c are determined by equations (23) and (24) in such a way that one considers the distributed charge $q_1(h_0)$ in the region of the axis $0 \leq h_0 \leq a$, to be united with an upper charge concentration point at $r = 0$; $h = c$.

$$Q_0 = \int_0^a q_1(h_0)\cdot dh_0 \quad (24)$$

$$c = \frac{1}{Q_0}\int_0^a \frac{q_1(h_0)\cdot h_0 \cdot dh_0}{Q_0} \quad (25)$$

The use of the tangential procedure, again enables the rewriting of the integrals (23) and (24) as a finite sum:

$$Q_0 = \Delta h_0 \sum_{n=\lambda/2+1}^{N} q_{1n} \quad (26)$$

$$c = \frac{\Delta h_0}{Q_0} \sum_{n=\lambda/2+1}^{N} q_{1n}\cdot h_{0n} \quad (27)$$

In the same manner, the charge distribution $q_1(h_0)$, in the region $-a \leq h_0 \leq 0$ of the radiator axis, should be concentrated about a lower charge concentration point. $r = 0$; $h = -c$.

Near the radiation axis, $x \approx 0$, the following approximation is found:

$$\phi_1 \approx \frac{Q_c}{4\pi\varepsilon_0}\left(\frac{1}{h_1+c} - \frac{1}{h_2+c}\right) \qquad (28)$$

One obtains a satisfactory distribution function $q_2(h_0)$ if one subtracts a correction term from the constant charge distribution q_0. This correction term is proportional to the potential ϕ_1 which is approximated by (28) and at the same time is also proportional to the distance h_0 from the ground plane. In this manner equation (29) is derived

$$q_2(h_0) = q_0 - d\, h_0\left(\frac{1}{h_1+c} - \frac{1}{h_2+c}\right) \qquad (29)$$

As can be seen from equation (23), ϕ_1 approaches 0 as q_0 goes to ∞. Therefore, $q_2(h_0)$ must approach the value q_0 asymptotically as h_0 increases. q_0 is specified by (13) through the handicap of a aperture angle $2\vartheta_c$ (10). The optimal value for the constant d can only be determined by trial and error.

The integral (9) is solvable in closed form for $q_2(h_0)$ by using the equation (29) and one obtains:

$$4\pi\varepsilon_0\Phi_2 = -q_0 \ln \frac{-(h-b)+\sqrt{r^2+(h-b)^2}}{h+b+\sqrt{r^2+(h+b)^2}} -$$

$$- \frac{d\cdot c}{\sqrt{r^2+(h-c)^2}} \left(\ln \frac{h-c+\sqrt{r^2+(h-c)^2}}{-(h-c)+\sqrt{r^2+(h-c)^2}} + \ln \frac{b+c}{b-c} + \right.$$

$$\left. + \ln \frac{(h-c)(h-b)+r^2+\sqrt{r^2+(h-b)^2}\sqrt{r^2+(h-c)^2}}{(h-c)(h+b)+r^2+\sqrt{r^2+(h+b)^2}\sqrt{r^2+(h-c)^2}} \right) +$$

$$+ \frac{d\cdot c}{\sqrt{r^2+(h+c)^2}} \left(\ln \frac{-(h+c)+\sqrt{r^2+(h+c)^2}}{h+c+\sqrt{r^2+(h+c)^2}} + \ln \frac{b+c}{b-c} + \right.$$

$$\left. + \ln \frac{(h+c)(h+b)+r^2+\sqrt{r^2+(h+b)^2}\sqrt{r^2+(h+c)^2}}{(h+c)(h-b)+r^2+\sqrt{r^2+(h-b)^2}\sqrt{r^2+(h+c)^2}} \right)$$

II.2.2 The Charge Distribution Function $q_1(h_0)$

If one retains for $q_1(h_0)$ (as in paragraph II,1) the originally calculated charge distribution for the finite radiator shape in its unchanged form and combines it with a line charge $q_2(h_0)$ according to (29) of the proper choice, then one actually obtains an equipotential line

$$\Phi = \Phi_1 + \Phi_2 = 2{,}0 \frac{q_1(h_0)}{4\pi\varepsilon_0}$$

Which runs out quickly enough in region B of Fig.18 into the prescribed extension cone of 1° aperture angle. However, since the effect of Φ_2 upon the line charge $q_2(h_0)$ is also noticeable in region A of Fig.18, the potential line

$$\Phi = 2{,}0 \frac{q_1(h_0)}{4\pi\varepsilon_0}$$

(similar to the line of equal potential in Fig.32) still has the disadvantage that it peels off too soon from the contor of the finite radiator. This disadvantage can be eliminated if the charge distribution $q_1(h_0)$ can be changed in such a way, that the corresponding potential Φ_1 upon the radiator surface does not have the form

$$\Phi_1 = 2{,}0 \frac{q_1(h_0)}{4\pi\varepsilon_0}$$

but takes on a new form according to

$$\Phi_1 = 2{,}0 \frac{q_1(h_0)}{4\pi\varepsilon_0} - \Phi_2$$

whereby the additional influence Φ_2 of the line charge $q_2(h_0)$ in part A of Fig.18 is just compensated for.

This changed line charge $q_1(h_0)$ can be calculated in accordance with the described iteration proceedure of [15], paragraph 4.2 with an electbonic digital computer. One must only assume the the desired form of the potential line

$$\Phi = \Phi_1 + \Phi_2 = 2{,}0 \frac{q_1(h_0)}{4\pi\varepsilon_0}$$

in region A of Fig 18 and calculate the potential ϕ_2 of the already known line charge $q_2(h_0)$ in N points of the described curve according to equation (30). Then the charge distribution $q_1(h_0)$ in the individual iteration steps is changed until the corresponding potential ϕ_1 has obtained the value

$$\Phi_1 = 2{,}0 \frac{q_1(h_0)}{4\pi\varepsilon_0} - \Phi_2$$

with considerable accuracy in these N points.

Result

Both charge distributions $q_1(h_0)$ and $q_2(h_0)$, for the 60 ohm spherical radiator having an infinite extension cone of 90° aperture angle, are shown in Fig. 33. The following values are to be used for the constants in equation (29)

$$q_0 = 0{,}784 \cdot q_1(0)$$

$$c = 0{,}7554$$

$$d = 1{,}304 \cdot q_1(0)$$

$$b = 1{,}508$$

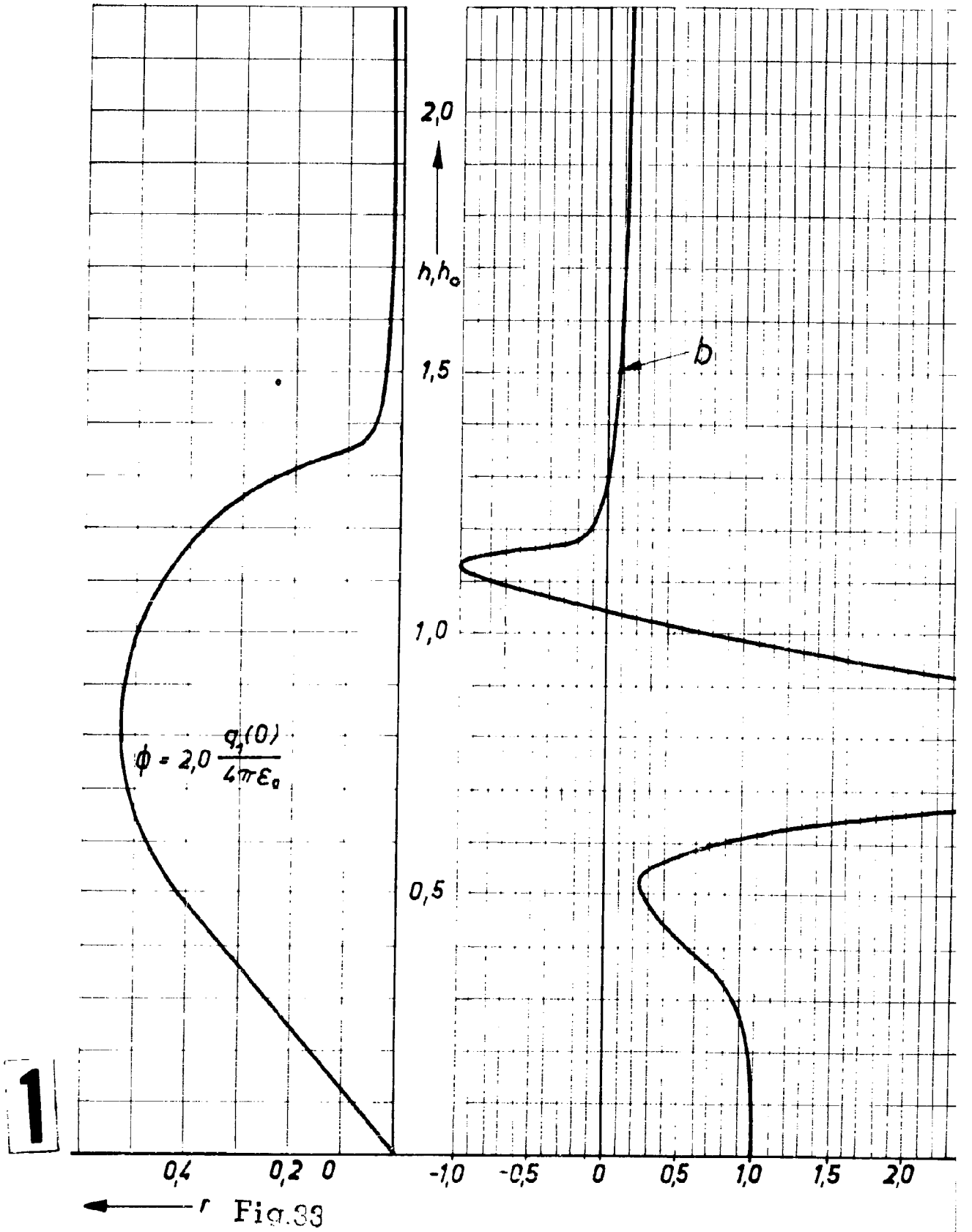
2,0
h, h₀
1,5
1,0
0,5
b
$\phi = 2{,}0 \frac{q_1(0)}{4\pi\varepsilon_0}$
0,4
0,2
0
-1,0
-0,5
0
0,5
1,0
1,5
2,0
r

1

Fig.33

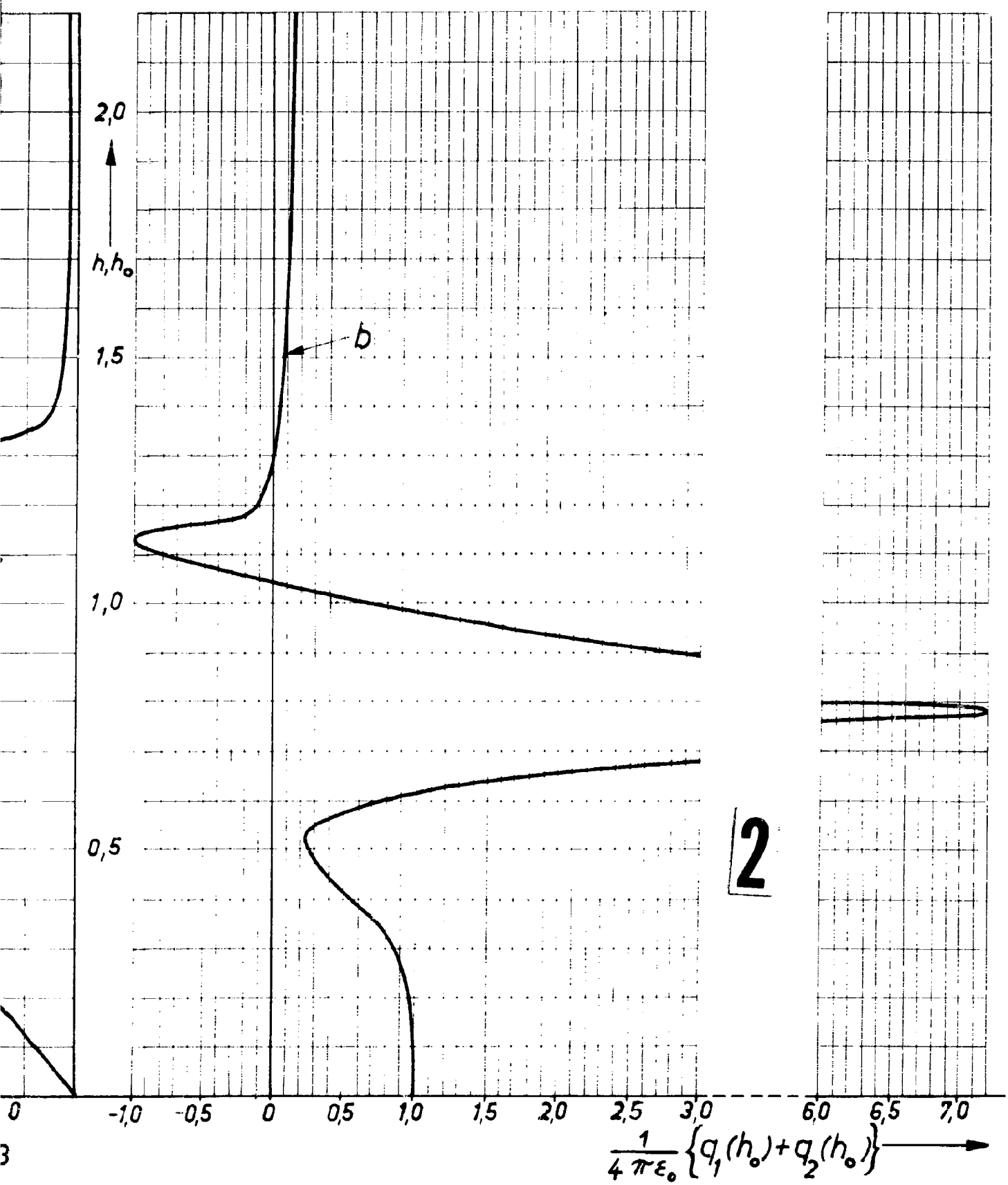
2,0
h, h₀
1,5
1,0
0,5
b
2
0
-1,0
-0,5
0
0,5
1,0
1,5
2,0
2,5
3,0
6,0
6,5
7,0
1/4πε₀ {q₁(h₀)+q₂(h₀)}

The potential line

$$\Phi = 2{,}0 \frac{q_1(h_0)}{4\pi\varepsilon_0}$$

is also drawn in Fig.33. This potential line does not show a noteworthy deviation from the desired shape

Future Plans

The other potentials $\phi = \phi_1 + \phi_2 = \text{constant}$ can also be easily calculated from the charge distribution $q_1(h_0) + q_2(h_0)$ with an electronic digital computer. Although the contract No AF 61 (051)-41 has terminated on 31 Jan. 1961, we have planned to continue, on our own, and solve the Maxwell equations for the new and better coordinate system for the 60 ohm spherical radiator in order to be able to explain the complete impedance and radiation behavior in a theoretical manner.

Bibliography:

1	H .Meinke	Zylindersymmetrische Breitband-Rundstrahler mit Hochpaß-Anpassung Nachrichtechn.Z. 13 (1960), S.162-168
2	W.Stöhr und O.Zinke	Wege zum optimalen Breitband-Rundstrahler Frequenz 14 (1960), S.26-35
3	H.Meinke	Die Stromverteilung auf Breitbandstrahlern und ihr Strahlungsdiagramm Nachrichtentechn.Fachber.23 (1961) . . .
4	H .Wolter	Strahlungsdämpfung, Widerstände und Richtdiagramme von Überbreitbandantennen Zeitschrift für angewandte Physik, IV, Bd., Heft 2 (1952), S.60-70
5	H.Meinke	Ein neuer Weg zur Lösung des Problems der Breitbandantenne NTZ 10 (1957), S.594-601
6	G.Joos	Lehrbuch der theoretischen Physik 10.Aufl.Frankfurt 1959, Kap9 und 10
7.	F.E.Ermann	Radio Engineers'Handbook, Mc Graw-Hill B.C. (1943), S.830
8	A.P.King	The radiation charakteristics of conical horn antennas IRE Proc.38, (1950), S.240-251
9	H.Meinke	Breitbandrichtantennen mit gutem Flächenwirkungsgrad Fernmeldetechn.Z. 7 (1954), S.161-170
10	S.Silver	Microwave antenna theory and disign, Chap. 6, Radiation Laboratory Series Mc Graw-Hill (1947)
11	W. Kleen	Einführung in die Mikrowellen-Elektronik Stuttgart 1952 18.Kap.
12	A.Knopf	Kleine Trichterantenne mit verbessertem Flächenwirkungsgrad Nachrichtentechn.Z.9 (1956), S.408-410

13	G.P.Robinson	Three-dimensional microwave lens Tele-Tech. November 1954, S.73 ff
14	A.Heilmann	Die günstigste Strom- oder Feldverteilung bei Flächen- und Längsstrahlern mit kontinuierlicher Belegung Nachrichtentechn. Z. (1956), S.1-9
15	F.J.Fuchs	Potentialfelder von Linienladungen als kreiszylindrisches Koordinatensystem für Strahlungsfelder von Breitbandantennen Dissertation, TH München 1959 Institut für Hochfrequenztechnik
16	R.W.Ealing	The theory of linear antennas Cambridge (USA) 1956
17	W.I.Smirnow	Lehrgang der höheren Mathematik Berlin 1956

UNCLASSIFIED